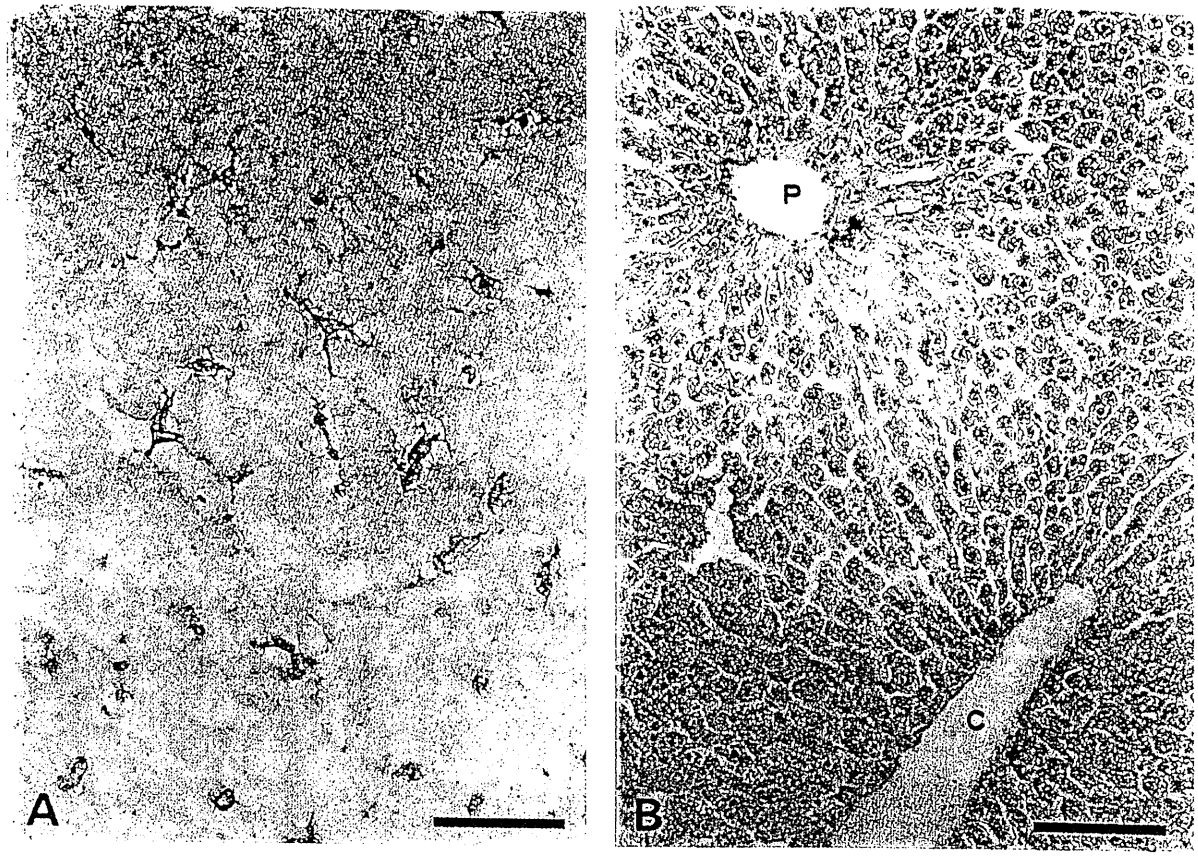

Figure 2. Expression of HO-1 and HO-2 in the normal rat liver. The 10-μm-thick sections were immunostained with GTS-1 (*A*) and GTS-2 (*B*). *P* and C denote portal and central venules, respectively. *Bars* represent 50 μm and 100 μm in *A* and *B*, respectively.

36 kD, respectively. We also examined adequacy of the use of these mAbs for Western blotting analysis using the tissue lysates collected from rats. Fig. 1 *C* illustrates representative data using spleen and testis, which are known to be abundant sources of HO-1 and HO-2, respectively (13, 31). As seen, GTS-1 and GTS-2 specifically recognized the presence of the two isoforms. These results indicate that, under both native and denatured conditions, these two mAbs can recognize their own counterpart antigen without displaying notable cross-reactivities.

Expression of HO-1 and HO-2 in the liver. Immunohistochemical analysis in the liver disclosed different topographic patterns in distribution of the two isozymes. First, HO-1 distributed in a relatively small number of cells that scattered over the entire lobule (Fig. 2 *A*). These HO-1–positive cells were characterized by their irregular and dendritic shapes, and by protrusion of their cytoplasm towards sinusoidal spaces, suggesting the presence of HO-1 in Kupffer cells. On the other hand, hepatocytes exhibited little staining, if any. By contrast, HO-2 occurred in the parenchymal cells and distributed homogeneously among the entire lobule, while nonparenchymal cells displayed practically no staining (Fig. 2 *B*). We examined the specificity of mAb binding to the corresponding antigens by preabsorbing with an excess of rHO-1 or rHO-2 protein, resulting in the absence of detectable immunostaining in each case (data not shown).

We further attempted to determine specific cell types that express HO-1 among the nonparenchymal cells. The HO-1 distribution in Kupffer cells was demonstrated by staining the same section simultaneously with GTS-1 and the antitissue macrophage mAb Ki-M2R. A majority of the cells stained dark brown, and indicated superimposition of the two colors; that is, light brown (GTS-1) and purple (Ki-M2R; Fig. 3 *A*). When hepatic stellate cells were stained purple with the anti-desmin Ab, it became clear that the HO-1–positive cells that were recognized as those stained brown were dissociated from desmin-positive cells, indicating that hepatic stellate cells exhibited little if any HO-1 staining (Fig. 3 *B*). These findings indicate that Kupffer cells constitute a major cellular compartment responsible for intrahepatic HO-1 expression.

Intrahepatic distribution of HO-1 exhibited quite different pictures when the liver was prestimulated with LPS, an inducer of this enzyme. The liver exposed to the 6-h pretreatment revealed that HO-1 not only occurred in tissue macrophages, but was also induced markedly in hepatocytes (Fig. 4 *A*). On the other hand, as seen in Fig. 4 *B*, HO-2 staining did not display any notable changes as compared with the control liver illustrated in Fig. 2 *B*. These results indicate that Kupffer cells and

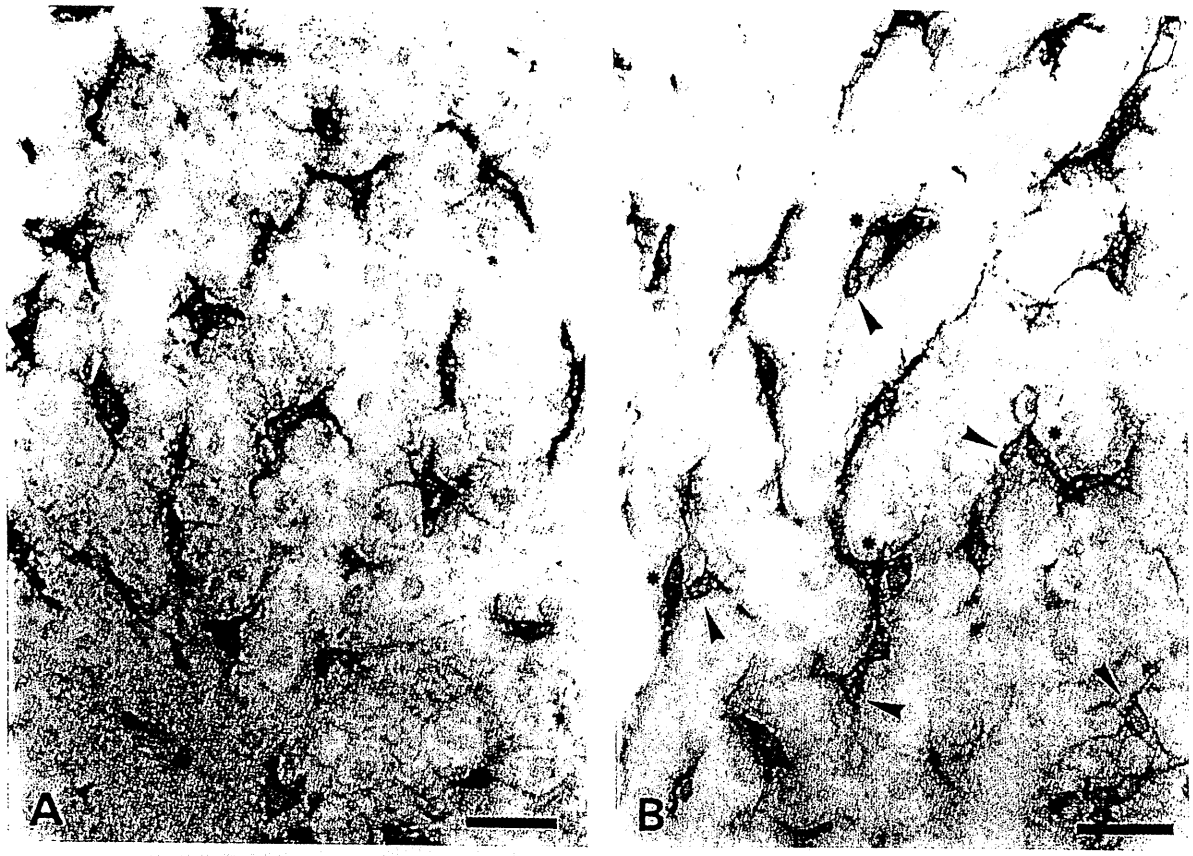

Figure 3. Characterization of nonparenchymal cells expressing HO-1 in the rat liver using the double immunohistochemical staining method. In *A*, the section was double-immunostained with GTS-1, an anti-rHO-1 mAb (*brown*), and with Ki-M2R, an mAb recognizing tissue macrophages (*light purple*). Colocalization of these two colors can be recognized by the *dark brown color*. In *B*, the section was stained with GTS-1 (*light brown, asterisks*) and then with an anti-desmin II mAb that recognizes hepatic stellate cells (*purple, arrows*). *Bar*, 50 μm in both panels.

hepatocytes constitute major cellular components that express the inducible HO isozyme in the endotoxin-treated liver.

CO generation in isolated hepatocytes. Table I shows the release of CO and bilirubin in isolated rat hepatocytes cultured in the double-lumen bioreactor. In the control, the rate of CO production in the hepatocytes was 27 nmol/h/10^8 cells during the initial 1-h period of incubation. When ZnPP was added in the medium at a final concentration of 1 μM, CO became undetectable, at least during the initial incubation period, showing that hepatocytes were able to generate CO through the heme oxygenase reaction. The average flux of CO from the hepatocyte suspension estimated on the basis of assumption that 1 g of wet liver tissue containing 1×10^8 hepatocytes (32) was ~ 0.45 nmol/min/g liver, indicating that the cellular CO flux is comparable to that determined in the venous perfusate collected from the perfused liver (10). These results suggest that hepatocytes constitute a major component for endogenous CO generation in the perfused liver.

Vasoconstrictive effects of free and liposome-encapsulated Hb in perfused liver. Fig. 5 illustrates time history of alterations in the whole organ vascular resistance elicited by administration of free HbO_2 or $HbV\text{-}O_2$ in perfused rat liver. As seen, immediately after the start of HbO_2 administration, the resistance increased markedly, showing a 25% elevation as compared with that in the steady-state conditions. When the perfusate was replaced by the Hb-free buffer at 15 min, the increased resistance decreased gradually and reached the control level at 30 min, indicating that the HbO_2-induced vascular response is reversible. On the other hand, metHb, a reagent that could scavenge NO but not CO, did not alter the vascular resistance, suggesting that CO plays a major role in lowering the

Table I. Production of CO by Isolated Rat Hepatocytes Cultured in a Double Lumen Bioreactor

Groups	CO
	nmol/h/10^8 hepatocytes
Control	27.5±5.0
ZnPP	3.8±0.8*

Data represent mean±SD of four separate experiments. The flux of CO and bilirubin was calculated from five separate experiments. *$P < 0.01$ as compared with the control values.

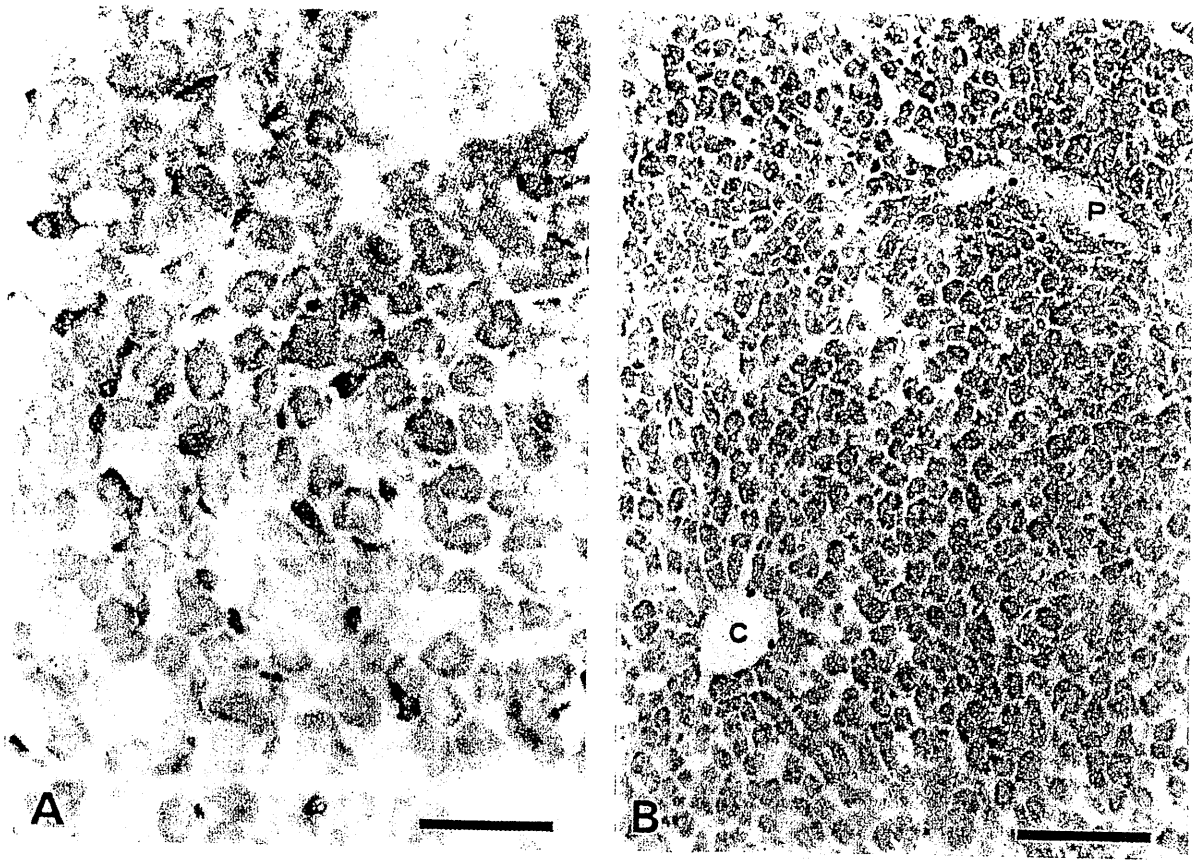

Figure 4. Immunohistochemical analysis of the expression of HO-1 and HO-2 in the liver sampled 6 h after treatment with intraperitoneal injection of lipopolysaccharide at 4 mg/kg. *A* and *B* illustrate the liver sections stained with GTS-1 and GTS-2, respectively. *Bars*, 50 μm and 100 μm in *A* and *B*, respectively. *P* and *C* denote portal and central venules, respectively.

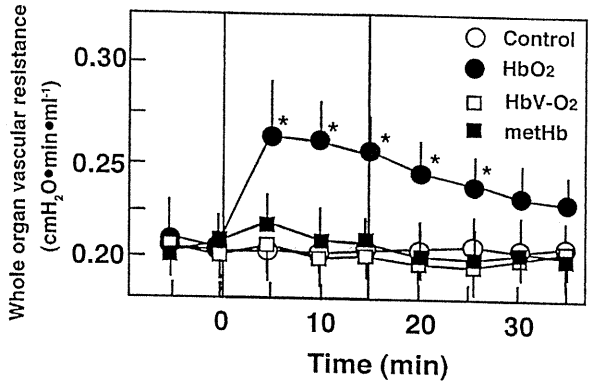

Figure 5. Time history showing effects of Hb derivatives on the whole organ vascular resistance in perfused rat liver. The Hb derivatives (HbO_2, HbV-O_2, metHb) were administered at a final Hb concentration of 1.5 g/dl for 15 min as seen in the shaded area. Data represent mean±SE of six experiments in each group. *Open* and *closed circles* indicate the data collected from the control and HbO_2-treated livers, respectively. *Open and closed squares* are those collected from the groups treated with HbV-O_2 and metHb, respectively. $*P < 0.05$ as compared with the data in the control group.

vascular resistance under the current experimental conditions. To specify the role of CO generated in intra- and extravascular compartments, effects of HbV-O_2 on the vascular resistance were examined. As seen, HbV-O_2 administration did not evoke any significant elevation in the resistance. These results suggest that HbO_2-induced elevation of the vascular resistance was abolished when diffusion of Hb across the sinusoidal endothelium into the space of Disse was blocked by its liposomal encapsulation.

We further examined the vascular responses at the level of hepatic sinusoids during the HbO_2 administration using laser confocal microangiography in the perfused liver (Fig. 6). Administration of HbO_2 induced a marked sinusoidal narrowing. The response was characterized by discontinuous patterns of narrowing in local sinusoidal segments colocalized with hepatic stellate cells that were able to be identified by vitamin A autofluorescence in their fat droplets. At the same time, several sinusoids exhibited continuous patterns of the decrease in their caliber. These findings were similar to those induced by ZnPP, a heme oxygenase inhibitor, as previously reported (10). Such a heterogeneous feature of the sinusoidal responses was confirmed by morphometrical analysis comparing changes in the diameter measured at local sinusoidal segments colocal-

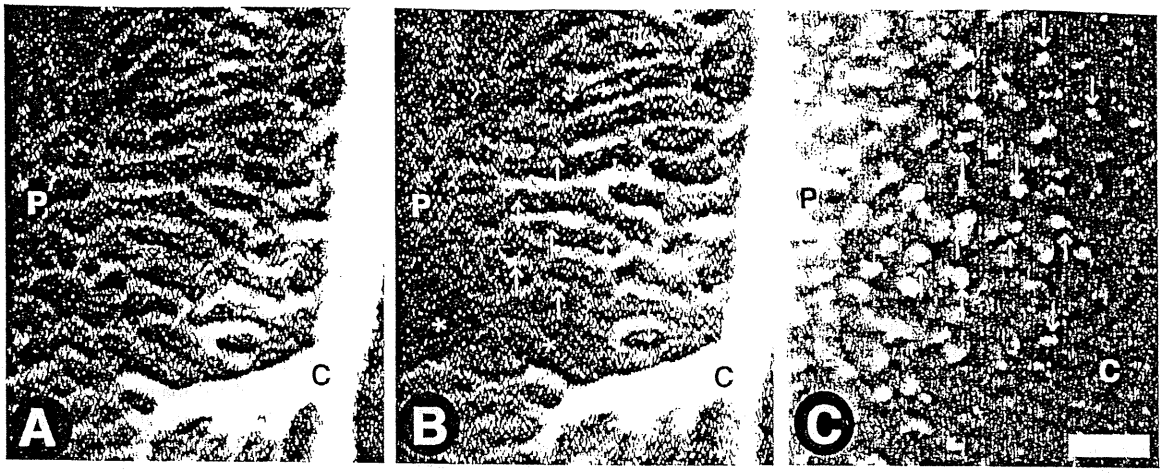

Figure 6. Representative microangiographs showing effects of HbO_2 on sinusoidal caliber in the perfused rat liver. The buffer solution containing FITC-labeled dextran was injected transportally before (*A*) and 5 min after the start of the HbO_2 administration (*B*) to visualize sinusoids. *C* illustrates distribution of vitamin A autofluorescence as a landmark of hepatic stellate cells in the same microscopic field. *P* and C denote portal and central venules, respectively. *Arrows* denote local sinusoidal segments displaying narrowing responses corresponding to localization of hepatic stellate cells, while *asterisks* indicate those displaying a continuous pattern of narrowing or lack in filling of the fluorochrome. *Bar*, 100 μm.

ized with hepatic stellate cells to those measured at the segments without the cells (Table II). HbO_2 administration induced an ~ 10–20% decrease in the diameter, preferentially at the local sinusoidal segments colocalized with the stellate cell–associated vitamin A autofluorescence. On the other hand, sinusoidal narrowing responses were not evident in the groups treated with HbV-O_2. These results suggest that hepatic sinusoids constitute a vascular component responsible for the HbO_2-elicited increase in the vascular resistance in perfused rat liver.

Discussion

The current study demonstrates for the first time that two distinct HO isoforms distribute in different kinds of cells in the liver: HO-1 in Kupffer cells, and HO-2 in parenchymal cells. We have recently shown that CO serves as an endogenous factor that actively lowers sinusoidal tone, and is necessary to guarantee ample blood supply into these vessels, in that elimination of CO by ZnPP, a potent inhibitor of heme oxygenase, evoked a marked increase in baseline vascular resistance (10). The vascular component responsible for the increasing resistance appears to involve sinusoids inasmuch as these vessels displayed a discontinuous pattern of narrowing in response to ZnPP administration. The ZnPP-elicited sinusoidal constriction is induced at least in part by the mechanisms involving hepatic stellate cells, microvascular pericytes occurring in the space of Disse (33) that are considered to be CO-sensing machinery for sinusoidal relaxation (10, 34). Importantly, supplementing CO at micromolar levels in the perfusate attenuated these changes elicited by ZnPP. These results suggest that stellate cells account for an important cellular target that can respond to endogenously generated CO. However, there has been little information about the intrahepatic cellular components responsible for CO generation and their anatomical proximity to the stellate cells.

Although the present findings show that Kupffer cells and hepatocytes constitute a major cellular source of HO, it remains unknown which cellular compartment plays a major role as an endogenous source of CO in the liver. According to the estimation of the CO flux determined in the isolated hepatocytes and its comparison to that in the perfused liver preparation, hepatocytes are likely to constitute a major cellular component for endogenous CO generation, and thus play an

Table II. Alterations in the Sinusoidal Caliber During Administration of HbO_2 and HbV-O_2 in Perfused Rat Liver

Groups	Sinusoidal caliber	
	0 min	5 min
	μm	μm
Control		
HSC (+)	10.9±0.9	11.1±0.7
HSC (−)	11.1±0.5	11.3±0.6
HbO_2		
HSC (+)	10.7±0.7	8.9±0.3*‡
HSC (−)	11.0±0.5	10.2±0.4§
HbV-O_2		
HSC (+)	10.3±0.5	10.2±0.4
HSC (−)	10.6±0.5	10.4±0.3

Data represents mean±SD of more than 60 measurements from 4 separate liver preparations. HSC (+) and HSC (−) denote local sinusoidal segments colocalized with and without hepatic stellate cells (HSC). Measurements were carried out from FITC-dextran microfluorographs captured before (0 min) and 5 min after starting the administration of Hb derivatives. *$P < 0.01$ as compared with the data collected from HSC (+) segments in the control group. ‡$P < 0.01$ as compared with the data collected from HSC (−) segments in the same group. §$P < 0.05$ as compared with the data measured at 0 min that were collected from HSC (−) segments in the same group.

important role for endogenous CO generation. Furthermore, our findings obtained by using Hb derivatives suggest that elimination of CO in the extrasinusoidal space (e.g, the space of Disse) causes a marked sinusoidal constriction. In contrast to microvascular endothelium of other organs, sinusoidal endothelium possesses abundant small pores called fenestration. Since the size of the pores is no greater than 200 nm in diameter (27), free Hb, but not HbV, has a free access to the space of Disse.

It was previously reported that systemic administration of inhibitors of NO synthase evokes sinusoidal constriction in mice in vivo (35). However, when the absence of vasoconstrictive action of metHb, which can trap NO but not CO (36), is considered, the role of endogenously generated NO is unlikely to play a role with the previous results, showing that inhibitors of NO synthase do not induce vasoconstrictive changes in the isolated perfused liver (10). Taking these circumstances into account, we suggest that free HbO_2 diffusing into the space of Disse eliminates CO in situ, and thereby evokes sinusoidal constriction.

In our earlier study, ZnPP was used to examine the role of CO in sinusoidal relaxation. It should be taken into account that ZnPP could increase the sinusoidal tone through direct inhibitory action on soluble guanylate cyclase (37) or inducible and neural NO synthases (38), or through activation of voltage-gated calcium channels (39). However, this possibility is unlikely to be involved (at least under our experimental conditions) when considering the following data: first, supplement of CO attenuated the ZnPP-induced increase in the resistance, and restored a reduction of tissue cGMP contents (11). Second, as discussed earlier, inhibitors of NO synthase did not increase the sinusoidal tone (10). Finally, we have recently shown that hepatic stellate cells in culture isolated from the intact liver exhibit little expression of the voltage-dependent Ca^{2+} channel (34). Furthermore, the present approach using different Hb derivatives that are able to eliminate or to maintain CO in situ without affecting the enzyme activity of HO convinced us that the action of ZnPP on sinusoidal tone is ascribable mainly to elimination of CO. There is still a possibility that the Hb derivatives per se exert vasoconstrictive actions through the CO-independent mechanisms such as stimulation of α-adrenergic receptors (40). However, the data illustrating distinct vasoconstrictive responses among HbO_2, metHb, and HbV, together with our previous finding that phenylephrine, an α_1 agonist, evokes constriction of portal vessels rather than sinusoids (10), leads us to suggest that involvement of such CO-independent mechanisms appear to be little, if any.

Considering the microanatomical orientation of the liver cells in and around sinusoids, HO-2 in hepatocytes stands in the reasonable position where the released CO can directly influence the contractile function of hepatic stellate cells located adjacent to the parenchymal region. On the other hand, CO released from HO-1 in Kupffer cells could easily be trapped by HbO_2 present in the circulating erythrocytes, and is therefore unlikely to exert its action on the stellate cells that occur in the extrasinusoidal space. In this context, at least in the ex vivo perfusion system, the current data show physiological significance of extrasinusoidal CO-mediated mechanisms for microvascular relaxation, and thus suggest that CO derived from HO-2 in the hepatocytes contributes to active relaxation of the sinusoids to a greater extent than that derived from HO-1 in Kupffer cells. It is, however, still unknown whether CO derived from HO-1 plays a role in regulation of sinusoidal tone under physiological conditions in vivo, since Kupffer cells can obtain greater amounts of heme substrates from the portal circulation (e.g., senescent erythrocytes). It should therefore be necessary to study whether these macrophages might use CO generated by HO-1 to control sinusoidal perfusion.

When the previously proposed mechanisms for intrahepatic heme degradation are taken into account, the present findings suggest a possible cooperative role of these two isoforms in catabolism of hemoglobin-derived heme in different cellular compartments. Namely, previous studies by Bissel et al. (41) revealed that removal of senescent erythrocytes from the circulation is carried out by macrophages in the liver and spleen, while hemoglobin released as a consequence of erythrocyte destruction can be metabolized mainly in the liver parenchyma. Spontaneous expression of the inducible HO isoform in Kupffer cells of the control liver appears to result from constant exposure of the cells to senescent erythrocytes in the sinusoidal compartment inasmuch as such an expression of HO-1 is evident as well in macrophages in red pulp of spleen, another major compartment for erythrocyte removal and heme degradation (2). On the other hand, the liver parenchyma is considered to be a major cellular compartment for localization of nonhemoglobin heme proteins, including cytochrome P450 (42). Since heme molecules of these enzymes are known to be metabolized exclusively by the heme oxygenase reaction (2), it is not unreasonable to suggest that, in the normal liver, HO-2 limits intrahepatic turnover of the heme enzymes.

Several studies have recently suggested a protective role of HO-1 induction against cell and tissue damages in that a decrease in free heme as well as an increase in bilirubin production help minimize oxidant-dependent cytotoxicity under disease conditions such as endotoxemia (43, 44). However, it is still unknown in the liver whether such HO-1–mediated upregulation in heme degradation is beneficial in protecting the tissue from oxidative stress. In conjunction with our recent observation that CO serves as a cholestatic factor (11), over expression of HO-1 may lead to hepatobiliary complications including hyperbilirubinemia and cholestasis, which could also occur clinically in endotoxemia (45, 46). Thus, pathophysiological significance of the inducible HO isozyme in the liver should be examined further under various disease conditions.

Acknowledgments

The authors thank Drs. Shinji Sakamoto, Katsunari Tedzuka, Tsuyoshi Sano, and Masaya Shiomi for technical assistance. We also thank the late Professor Emeritus Benjamin W. Zweifach for his suggestion to prepare the manuscript.

This work was supported by Grant-in-Aid for Scientific Research from the Ministry of Education, Science, and Culture of Japan (09470143, 07508005), and by grants from Keio University School of Medicine, Research Foundation for Opto-Science and Technology, and in part by Surveys and Research on Specific Diseases from the Ministry of Health (1996 and 1997). Nobuhito Goda is a research fellow supported by the Japan Society for the Promotion of Science in 1997.

References

1. Shibahara, S., R. Müller, H. Taguchi, and T. Yoshida. 1985. Cloning and expression of cDNA of rat heme oxygenase. *Proc. Natl. Acad. Sci. USA* 82:

7865–7869.

2. Maines, M.D. 1988. Heme oxygenase: function, multiplicity, regulatory mechanisms, and clinical applications. *FASEB J.* 2:2557–2568.

3. Ewing, J.F., and M.D. Maines. 1991. Rapid induction of heme oxygenase 1 mRNA and protein by hyperthermia in rat brain: heme oxygenase 2 is not a heat shock protein. *Proc. Natl. Acad. Sci. USA.* 88:5364–5368.

4. Rizzardini, M., M. Terao, F. Falciani, and L. Cantoni. 1993. Cytokine induction of haem oxygenase mRNA in mouse liver. *Biochem. J.* 290:343–347.

5. Maines, M.D., and A. Kappas. 1977. Metals as regulators of heme metabolism: physiological and toxicological implications. *Science.* 198:1215–1221.

6. Kurata, S., M. Matsumoto, Y. Tsuji, and H. Nakajima. 1996. Lipopolysaccharide activates transcription of the heme oxygenase gene in mouse M1 cells through oxidative activation of nuclear factor κB. *Eur. J. Biochem.* 239:566–571.

7. Tacchini, L., L. Schiaffonati, C. Pappalardo, C. Gatti, and A. Bernelli-Zazzera. 1993. Expression of HSP 70, immediate-early response and heme oxygenase genes in ischemia-reperfused rat liver. *Lab. Invest.* 68:465–471.

8. Cruse, I., and M.D. Maines. 1988. Evidence suggesting that the two forms of heme oxygenase are products of different genes. *J. Biol. Chem.* 263:3348–3353.

9. Suematsu, M., S. Kashiwagi, T. Sano, N. Goda, Y. Shinoda, and Y. Ishimura. 1994. Carbon monoxide as an endogenous modulator of hepatic vascular perfusion. *Biochem. Biophys. Res. Commun.* 205:1333–1337.

10. Suematsu, M., N. Goda, T. Sano, S. Kashiwagi, Y. Shinoda, and Y. Ishimura. 1995. Carbon monoxide: an endogenous modulator of sinusoidal tone in the perfused rat liver. *J. Clin. Invest.* 96:2431–2437.

11. Sano, T., M. Shiomi, M. Wakabayashi, Y. Shinoda, N. Goda, T. Yamaguchi, Y. Nimura, Y. Ishimura, and M. Suematsu. 1997. Endogenous carbon monoxide suppression stimulates bile acid-dependent biliary transport in perfused rat liver. *Am. J. Physiol.* 272(35):G1268–G1275.

12. Stocker, R., A.N. Glazer, and B.N. Ames. 1987. Antioxidant activity of albumin-bound bilirubin. *Proc. Natl. Acad. Sci. USA.* 84:5918–5922.

13. Yamaguchi, T., F. Horio, T. Hashizume, M. Tanaka, S. Ikeda, A. Kakinuma, and H. Nakajima. 1995. Bilirubin is oxidized in rats treated with endotoxin and acts as a physiological antioxidant synergistically with ascorbic acid in vivo. *Biochem. Biophys. Res. Commun.* 214:11–19.

14. Oshio, C., and M.J. Phillips. 1981. Contractility of bile canaliculi: implications of liver function. *Science.* 212:1041–1042.

15. Rotenberg, M.O., and M.D. Maines. 1990. Isolation, characterization and expression in Escherichia coli of a cDNA encoding rat heme oxygenase-2. *J. Biol. Chem.* 265:7501–7506.

16. Ohashi, H., K. Maruyama, Y. Liu, and A. Yoshimura. 1994. Ligand-induced activation of chimeric receptors between the erythropoietin receptor and receptor tyrosine kinases. *Proc. Natl. Acad. Sci. USA.* 91:158–162.

17. Suda, T., T. Takahashi, P. Golstein, and S. Nagata. 1993. Molecular cloning and expression of the Fas ligand, a novel member of the tumor necrosis factor family. *Cell.* 75:1169–1178.

18. Yoshida, T., and G. Kikuchi. 1978. Reaction of the microsomal heme oxygenase with cobaltic protoporphyrin IX, an extremely poor substrate. *J. Biol. Chem.* 253:8479–8482.

19. McKinney, M.M., and A. Parkinson. 1987. A simple, nonchromatographic procedure to purify immunoglobulins from serum and ascites fluid. *J. Immunol. Methods.* 96:271–278.

20. Yamamoto, T., M. Naito, H. Moriyama, H. Umezu, H. Matsuo, H. Kiwada, and M. Arakawa. 1996. Repopulation of murine Kupffer cells after intravenous administration of liposome-encapsulated dichloromethylene diphosphonate. *Am. J. Pathol.* 149:1271–1286.

21. Yamaguchi, T., Y. Wakabayashi, M. Tanaka, T. Sano, H. Ishikawa, H. Nakajima, M. Suematsu, and Y. Ishimura. 1996. Taurocholate induces directional transport of bilirubin into bile in the perfused rat liver. *Am. J. Physiol.* 270:G1028–G1032.

22. Falkenberg, F.W., H. Weichert, M. Krane, I. Bartels, M. Palme, H.O. Nagels, and H. Fiebig. 1995. In vitro production of monoclonal antibodies in high concentration in a new and easy to handle modular minifermentor. *J. Immunol. Methods.* 179(1):13–29.

23. Sakai, H., S. Takeoka, H. Yokohama, Y. Seino, H. Nishide, and Y. Tsuchida. 1993. Purification of concentrated hemoglobin using organic solvent and heat treatment. *Prot. Expr. Pur.* 4:563–569.

24. Sakai, H., K. Hamada, S. Takeoka, H. Nishide, and E. Tsuchida. 1996. Physical properties of hemoglobin vesicles as red cell substitutes. *Biotechnol. Prog.* 12:119–125.

25. Rudolph, A.S., H. Spielberg, B.J. Spargo, and N. Kossovsky. 1995. Histopathologic study following administration of liposome-encapsulated hemoglobin in the normovolemic rats. *J. Biomed. Mater. Res.* 29:189–196.

26. Naito, M., and E. Wisse. 1978. Filtration effect of endothelial fenestrations on chylomicron transport in neonatal rat liver sinusoids. *Cell Tissue Res.* 190:371–382.

27. Wisse, E., R.B. DeZanger, K. Charels, P. van der Smissen, and R.S. McCuskey. 1985. The liver sieve: considerations concerning the structure and function of endothelial fenestrae, the sinusoidal wall and the space of Disse. *Hepatology.* 5:683–692.

28. Stock, R.J., E.V. Cilento, and R.S. McCuskey. 1989. A quantitative study of fluorescein isothiocyanate-dextran transport in the microcirculation of the isolated perfused rat liver. *Hepatology.* 9:75–82.

29. Iigou, Y., M. Suematsu, T. Higashida, J. Oheda, K. Matsumoto, Y. Wakabayashi, Y. Ishimura, M. Miyasaka, and T. Takashi. 1997. In vivo constitutive expression of ICAM-1 in rat microvascular systems analyzed by laser confocal microscopy. *Am. J. Physiol.* 273:H138–H147.

30. Suematsu, M., M. Oda, H. Suzuki, H. Kaneko, N. Watanabe, T. Furusho, S. Masushige, and M. Tsuchiya. 1993. Intravital and electron microscopic observation of Ito cells in rat hepatic microcirculation. *Microvasc. Res.* 46:28–42.

31. Ewing, J.F., and M.D. Maines. 1995. Distribution of constitutive (HO-2) and heat-inducible (HO-1) heme oxygenase isozymes in rat testes: HO-2 displays stage-specific expression in germ cells. *Endocrinology.* 136:2294–2302.

32. Knook, D.L., and A.M. De Leeuw. 1982. Connective tissue of the normal and fibrotic human liver. Thieme, Stuttgart. 67–71 pp.

33. Wake, K. 1980. Perisinusoidal stellate cells (fat-storing cells, interstitial cells, lipocytes), their related structure in and around the liver sinusoids, and vitamin A-storing cells in extrahepatic organs. *Int. Rev. Cytol.* 66:303–353.

34. Kashiwagi, S., M. Suematsu, Y. Wakabayashi, N. Kawada, M. Tachibana, A. Koizumi, M. Inoue, Y. Ishimura, and A. Kaneko. 1997. Electrophysiological characterization of cultured hepatic stellate cells in rats. *Am. J. Physiol.* 272 (35):G742–G750.

35. Nishida, J., R.S. McCuskey, D. McDonnell, and E.S. Fox. 1994. Protective role of NO in hepatic microcirculatory dysfunction during endotoxemia. *Am. J. Physiol.* 267:G1135–G1141.

36. R.F. Eich, T. Li, D.D. Lomon, D.H. Doherty, S.R. Curry, J.F. Aitken, A.J. Mathews, K.A. Johnson, R.D. Smith, G.N. Phillips, and J.S. Olson. 1996. Mechanism of NO-induced oxidation of myoglobin and hemoglobin. *Biochemistry.* 35:6976–6983.

37. Ignarro, L.J., B. Barrot, and K.S. Wood. 1984. Regulation of soluble guanylate cyclase activity by porphyrins and metalloporphyrins. *J. Biol. Chem.* 259:6201–6207.

38. Wolff, D.J., R.A. Naddelman, A. Lubeskie, and D.A. Saks. 1996. Inhibition of nitric oxide synthase isoforms by porphyrins. *Arch. Biochem. Biophys.* 333:27–34.

39. Linden, D.J., K. Narasimhan, and D. Gurfel. 1993. Protoporphyrins modulate voltage-gated Ca current in AtT-20 pituitary cells. *J. Neurophysiol.* 70:2673–2677.

40. Gulati, A., and A.C. Sharma. 1994. Prazosin blocks the pressor but not the regional circulatory effects of diaspirin crosslinked hemoglobin. *Life Sci.* 55: 121–130.

41. Bissell, D.M., L. Hammaker, and R. Schmid. 1972. Hemoglobin and erythrocyte catabolism in rat liver: the separate roles of parenchymal and sinusoidal cells. *Blood.* 40:812–822.

42. Kutty, R.K., R.F. Daniel, D.E. Ryan, W. Levin, and M.D. Maines. 1988. Rat liver cytochrome P-450*b*, P-420*b*, and P-420*c* are degraded to biliverdin by heme oxygenase. *Arch. Biochem. Biophys.* 260:638–644.

43. Choi, A.M.K., and J. Alam. 1996. Heme oxygenase-1: function, regulation, and implication of a novel stress-inducible protein in oxidant-induced lung injury. *Am. J. Respir. Cell Mol. Biol.* 15:9–19.

44. Camhi, S.L., J. Alam, L. Otterbein, S.L. Sylvester, and A.M.K. Choi. 1995. Induction of heme oxygenase-1 gene expression by lipopolysaccharide is mediated by AP-1 activation. *Am. J. Respir. Cell Mol. Biol.* 13:387–398.

45. Roelofsen, H., C.N. Van Der Veere, R. Ottenhoff, B. Schoemaker, P.L.M. Jansen, and R.P.J. Oude Elferink. 1994. Decreased bilirubin transport in the perfused liver of endotoxemic rats. *Gastroenterology.* 107:1075–1084.

46. Roelofsen, H., B. Schoemaker, R. Ottenhoff, P.L.M. Jansen, and R.P.J. Oude Elferink. 1995. Impaired hepatocanalicular organ anion transport in endotoxemic rats. *Am. J. Physiol.* 269:G427–G434.

Nitric Oxide Suppression Reversibly Attenuates Mitochondrial Dysfunction and Cholestasis in Endotoxemic Rat Liver

MASAYA SHIOMI,[1] YOSHIYUKI WAKABAYASHI,[2] TSUYOSHI SANO,[1] YUICHI SHINODA,[2] YUJI NIMURA,[1] YUZURU ISHIMURA,[2] AND MAKOTO SUEMATSU[2]

This study aimed to examine whether nitric oxide (NO) plays a causal role in endotoxin-induced dysfunction of biliary transport. Rats were treated with intraperitoneal injection of endotoxin (O111B4, 4 mg/kg). At 2 hours, the liver was excised and perfused *ex vivo* with taurocholate (TC)-containing Krebs-Ringer solution under monitoring bile output and NO_2 in the perfusate and tissue cyclic guanosine monophosphate (cGMP) levels as indices of NO production. The endotoxin treatment evoked a marked decrease in the bile acid–dependent bile formation concurrent with the increasing NO_2 output, cGMP elevation, and a reduction of hepatic adenosine triphosphate (ATP) contents and oxygen consumption. Perfusion with 1 mmol/L aminoguanidine (AG), an inhibitor of inducible NO synthase, but not with L-nitroarginine methyl ester, an inhibitor of the constitutive form of the enzyme, significantly reversed the endotoxin-induced increment of the bile formation in concert with the recovery of oxygen consumption and ATP levels. Laser confocal microfluorography of the liver lobules using rhodamine 123 (Rh), a fluoroprobe sensitive to mitochondrial membrane potential, revealed that endotoxin elicited a significant mitochondrial dysfunction panlobularly. The AG administration reversed the endotoxin-induced decrease in mitochondrial membrane potential. Collectively, up-regulation of NO by inducible NO synthase accounts for a mechanism through which endotoxin impairs the bile formation, and its suppression serves as a therapeutic strategy for improvement of hepatobiliary function. (HEPATOLOGY 1998;27:108-115.)

Nitric oxide (NO) is a gaseous mediator with diverse biological actions, and is thought to modify organ function in various disease conditions. In the liver, several studies have shown NO to be protective by acting as a vasodilator that minimizes an impairment of sinusoidal blood perfusion.[1,2] On the other hand, it was suggested that NO can play an active role in the pathogenesis of hepatobiliary disorders caused by ischemia/reperfusion injury or endotoxemia.[3,4] Current studies have provided evidence that the inducible form of NO synthase, the expression of which is up-regulated in the liver in response to cytokines and endotoxin,[5] contributes to the formation of peroxynitrite and hydroxyl radicals, and thereby causes the irreversible cell injury as assessed by histology and the release of enzymes from parenchymal cells.[6] These observations suggest a possible pathogenic role of NO overproduction in endotoxin-induced liver injury.

Despite these reports proposing a cytotoxic action of NO, little is known as to whether NO can exert its biological actions to evoke functional alterations in the liver without leading to irreversible cell damage. Bile formation is one of the most important functions of the liver that can be impaired by endotoxemia through NO-mediated mechanisms.[7,8] NO is known to stimulate cyclic guanosine monophosphate (cGMP) generation[9] and to inhibit bile canalicular contraction in cultured hepatocyte couplets.[10] It was also shown in the perfused rat liver that exogenously administered 8Br-cGMP, a membrane-permeable form of a cGMP analogue, stimulates bile acid-independent bile formation.[11] On the other hand, recent observations *in vitro* suggested that NO evokes mitochondrial dysfunction through its biological actions on enzymes containing the 4Fe-4S clusters, aconitase and succinate dehydrogenase,[9] or cytochrome *c* oxidase, an enzyme constituting the distal end of the mitochondrial respiratory chain.[12] Considering that maintenance of mitochondrial function and intracellular adenosine triphosphate (ATP) levels could dictate biliary function,[13] these facts lead us to hypothesize that endotoxin functionally impairs mitochondrial respiration and bile excretion through the mechanisms involving the overproduction of NO. The present study thus aimed to show that NO-dependent functional alterations actually occur in the endotoxemic liver. To this end, we have examined the effects of posttreatment of aminoguanidine (AG), an inhibitor of inducible NO synthase, on the endotoxin-elicited mitochondrial dysfunction and bile excretion, because reversibility of the liver dysfunction by NO suppression serves as a key to establish the clinical relevance of the enzyme activity as a potentially therapeutic target.

MATERIALS AND METHODS

Animal Preparation and Endotoxin Treatment. Male Wistar rats (range, 300-320 g) allowed free access to laboratory chow and tap water

Abbreviations: NO, nitric oxide; cGMP, cyclic guanosine monophosphate; ATP, adenosine triphosphate; AG, aminoguanidine; LPS, lipopolysaccharide; TC, taurocholate; MB, methylene blue; Rh, rhodamine 123.

From the [1]First Department of Surgery, Nagoya University School of Medicine, Nagoya, and [2]Department of Biochemistry, School of Medicine, Keio University, Tokyo, Japan.

Received April 17, 1997; accepted August 29, 1997.

A preliminary account pertinent to a portion of this work was presented at the Annual Meeting of the American Society for the Study of the Liver Diseases, November 1996, Chicago, IL.

Supported by a Grant-in-Aid for Scientific Research from the Ministry of Education, Science, and Culture of Japan, and by grants from Keio Medical Research Funds and from Sasagawa Research Foundation. Also supported in part by Surveys and Research on Specific Diseases from the Ministry of Health on 1997.

Address reprint requests to: Makoto Suematsu, M.D., Ph.D., Associate Professor, Department of Biochemistry, School of Medicine, Keio University, 35 Shinanomachi, Shinjuku-ku, Tokyo 160, Japan. Fax: 81-3-3358-8138.

0270-9139/98/2701-0018$3.00/0

were fasted 24 hours before experiments. Lipopolysaccharide (LPS) (O-111B4, Sigma, St. Louis, MO) was dissolved in physiological saline and intraperitoneally injected at 4 mg/kg, a dose that neither evoked significant increase in serum alanine transaminase nor induced histologically detectable necrotic changes over 6 hours. Two hours after the LPS treatment, the animals were anesthetized with pentobarbital sodium (50 mg/kg intraperitoneally) to prepare the isolated perfused livers as described previously.[14,15] Briefly, the distal portion of common bile duct was cannulated with a polyethylene catheter (PE-10) for biliary drainage, and the liver was perfused with Krebs-Ringer solution (pH 7.4, 37°C) gassed with carbogen (95% O_2, 5% CO_2) at a constant flow rate (4.0 mL/min/g liver weight) in a single-pass mode. The perfusion pressure was continuously monitored to estimate the vascular resistance as the ratio between the pressure gradient and flow rate.[16]

Experimental Groups Studied. To maintain physiological levels of bile output, all livers were perfused with the Krebs solution containing sodium taurocholate (TC), a major conjugated bile acid in rats, at 30 μmol/L (which is a concentration compatible with that determined in the portal circulation[14]) unless mentioned. In all experiments, L-arginine was added in the perfusion buffer at 50 μmol/L, a concentration equivalent to that in the rat blood samples.[6] Five main protocols were employed in the perfusion experiments. Livers in the first group were of the control perfused with the buffer containing sodium TC for 60 minutes. Namely, TC was infused continuously, and, when the flow rate was stabilized 20 minutes later, bile samples were collected every 5 minutes during the following 40 minutes. In the second, the LPS-treated liver was perfused according to the same protocol as that of the first group. The other three groups were prepared to evaluate the effects of exogenous supplement with the following interventions on the LPS-treated liver: 1 mmol/L AG, an inhibitor of inducible NO synthase, 1 mmol/L AG plus a lipophilic cGMP analogue, 8Br-cGMP (1 μmol/L; Sigma, St. Louis, MO), and 250 nmol/L methylene blue (MB), an inhibitor of guanylate cyclase. In some experiments, 1 mmol/L of N^{ω}-nitro-L-arginine methyl ester, a constitutive NO synthase inhibitor, was also used. The concentration of AG used in the current study was sufficient to abolish inducible levels of NO_2^- in the venous effluent collected from the LPS-pretreated liver, as shown later. In addition, 1 μmol/L of 8Br-cGMP was the smallest concentration that significantly suppressed the AG-induced biliary responses without altering the baseline vascular resistance. These reagents were added in the perfusate after completing the 20-minute stabilizing period. In separate experiments, time history of the bile output was traced in the absence of TC between the LPS-treated and control livers.

Measurements of Bile Output, Bile Acids, Phospholipids, and Bilirubin in Bile. Bile flow rate was expressed in microliters per minute per gram of liver as described previously.[14] Concentrations of total bile acids and phospholipids in the bile were determined using enzyme assay kits (Enzabile-2, Dai-ichi Chemicals, Tokyo, Japan; Phospholipid C-Test, Wako, Tokyo, Japan), respectively.[15]

Measurements of NO_2^- in the Hepatic Venous Perfusate. As an index of NO generation in the liver, concentrations of NO_2^- in the hepatic venous perfusate were determined by a fluorescence spectrophotometry based on the reaction of nitrite with 2,3-diaminonaphthalene to form the fluorescent product, 1-(H)-naphthotriazole, as described elsewhere.[17] Calibration curves were established by examining the fluorescence intensity in the presence of known concentrations of $NaNO_2$. Fluorescence measurements at 450 nm were performed under an excitation wavelength of 365 nm using a fluorescence spectrophotometer (F-3000, Hitachi, Co., Hitachi, Japan). This method allowed us to obtain the linearity between the concentrations of $NaNO_2$ and the fluorescence intensity in a range between 10 nmol/L and 500 nmol/L.

Determination of cGMP and ATP in the TC-Treated Perfused Liver. Tissue samples to determine cGMP were prepared from liver pieces excised and snap-frozen in liquid nitrogen after 60 minutes of perfusion (20-minute stabilizing perfusion followed by 40-minute perfusion). The liver was similarly snap-frozen in liquid nitrogen. cGMP was extracted using a solution of 0.1 mol/L perchloric acid at 0°C, and was determined by enzyme-linked immunoassay using assay kits (RPN225, Amersham, Arlington Heights, IL), respectively, as described elsewhere.[15] The same samples extracted from the liver tissue were also used to examine tissue ATP contents as an index of the viability of perfused livers. The ATP contents were determined by the luciferin/luciferase method using a multiwell microplate chemiluminescence analyzer (Dia-Iatoron Inc., Tokyo, Japan), as described elsewhere.[18]

Rhodamine 123-Assisted Digital Confocal Microfluorography in the Perfused Liver. Intrahepatic mitochondrial function was visually assessed in each experimental group by microfluorography using rhodamine 123 (Rh), a functional fluoroprobe that can bind mitochondria mainly in parenchymal hepatocytes in proportion to the inner membrane potential.[19,20] The isolated liver perfused with the 30-μmol/L TC-containing Krebs-Ringer buffer was loaded with Rh according to the previous experimental protocol with modifications.[16] The liver was first perfused for 10 minutes with the buffer containing Rh at 0.8 μmol/L, the concentration of which did not influence the baseline oxygen consumption.[20] The liver was then prepared with the continuous perfusion in the presence of the same concentration of TC and 0.2 μmol/L Rh to equilibrate the liver mitochondria with Rh. This supplementary dose of Rh was necessary to obtain the constant time history of Rh fluorescence intensity on the surface of the control livers, as well as those pretreated with LPS during the entire experiments (40 minutes). These procedures for Rh loading were performed by placing the liver on a specially designed plastic stage with a window made of a nonfluorescence cover glass. The hepatic Rh-associated fluorographs were obtained by an inverted-type intravital microscope (TMD-300, Nikon, Tokyo, Japan) equipped with a digital laser scanning confocal imaging system (Insight, Meridian Far East, Tokyo, Japan) under epi-illumination at 488 nm using the Argon laser power supply at 30 mW. This system allowed us to collect the confocal fluorescence images at a video-rate speed (30 frames/sec), and they were optically sliced with desired widths ranging between 1 μm and 20 μm. In the present study, the hepatic Rh fluorescence images were optically sliced with 2 μm, unless mentioned. The confocal Rh microfluorographs were visualized by a silicon-intensified target camera (C-2400-08, Hamamatsu Photonics, Hamamatsu, Japan) every 10 minutes after the start of experiments. At the end of experiments, fluorescein isothiocyanate–labeled albumin was injected transportally to establish the landmarks of the lobules such as terminal portal and central venules in the microscopic fields of interests.[21]

Separately, livers of the LPS-treated rats were loaded with the Krebs buffer containing 0.8 μmol/L Rh, and were then perfused with 1 mmol/L AG for 20 minutes without 0.2 μmol/L Rh. Evaluation of the Rh microfluorographs recorded under these protocols enabled us to check whether effects of the NO synthase inhibitor, if any, could be reproduced in the absence of the supplementary dose of Rh. Additionally, some livers exposed to LPS were perfused first with 1 mmol/L AG for 20 minutes and were then loaded with 0.8 μmol/L Rh for 10 minutes. By determining the intrahepatic Rh fluorescence under these protocols, we attempted to examine whether kinetics of the dye loading *per se* differs between the control and LPS-pretreated livers.

To examine intracellular distribution of the Rh loading in cultured hepatocytes, the cells were isolated from livers of the rats treated with or without the LPS administration according to the previous method.[22] The cells were treated with the Krebs buffer containing 0.8 μmol/L Rh for 10 minutes and washed twice with the Rh-free buffer. The Rh-loaded cells on the culture dish were observed through a 100× oil-immersion objective lens using the same confocal microscopic system.

The fluorescence images were digitally processed and introduced into an eight-bit computer-assisted image processor (Image 1.58/Power Macintosh 8100). To perform the data calibration, the Krebs buffer containing known concentrations (0.1 μmol/L-20 μmol/L) of

Rh were placed in the culture dishes mounted with the same fluorescence-free cover glass as that used to collect the hepatic microfluorographs. The relationship between the gray levels and the Rh concentrations was then established. Assuming that the Rh concentrations measured in the solution were equivalent to those measured on the liver surface, the gray level intensities of the hepatic Rh fluorescence (1-256) in different portions of lobules were expressed as apparent Rh concentrations (Rh_{app}) based on the calibration curve. Measurements of Rh_{app} were performed in different portions of the hepatic lobules, including periportal, midzonal, and pericentral regions using a variable window for the gray-level measurements according to our previous methods.[20,23]

Statistical Analysis. All data in the present study were expressed as mean ± SE of measurements. Differences in the mean values among the groups were analyzed by one-way ANOVA combined with a Scheffe-type multiple comparison test. $P < .05$ was considered statistically significant.

RESULTS

LPS-Induced Reduction of Bile Output and Its Reversal by AG. Figure 1 shows the time history of bile output in the control and LPS-pretreated livers. In the control liver, the baseline level of the bile output was approximately 2.5 μL/min/g liver during the entire course of observation. In the liver isolated from the rats that were exposed to the 2-hour LPS treatment, the baseline bile output became significantly lower, being approximately 70% of the control. The baseline output was gradually decreased in a time-dependent manner during the 40-minute observation period. The magnitude of the decrease in the baseline bile output became further decreased when endotoxin treatment was extended to 6 hours. When the livers were exposed to 2-hour or 6-hour endotoxin pretreatment, administration of 1 mmol/L AG significantly reversed the decrease in the baseline bile output, reaching a level comparable with that in the LPS-untreated group within 10 minutes. By contrast, such reversible responses were not observed when 1 mmol/L N^{ω}-nitro-L-arginine methyl ester was administered in the perfusate. As seen in the inset of Fig. 1, the 2-hour LPS pretreatment evoked a 25% decrease in the oxygen consumption as compared with that in the control liver. In the both groups, the baseline values were not changed during the observation period. When 1 mmol/L AG was administered in the LPS-pretreated liver, the oxygen consumption increased rapidly and reached a plateau level within 15 minutes after the start of the AG administration.

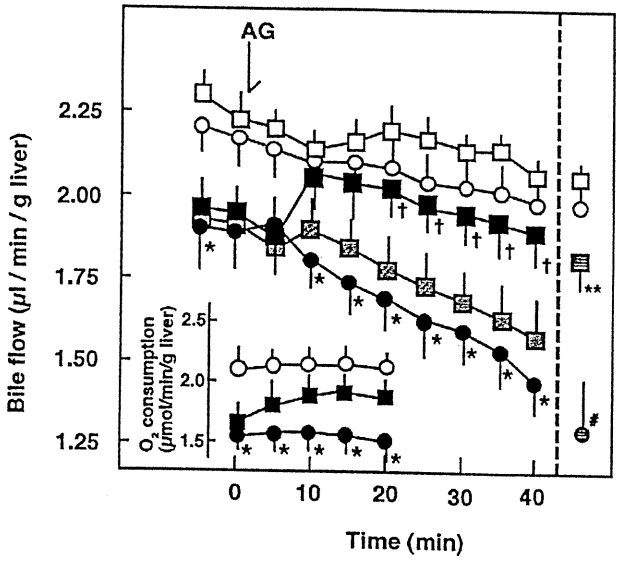

FIG. 1. Time history of bile output in the control perfused rat liver and that pretreated with endotoxin. (○ and ●) Data collected from the control and 2-hour LPS-treated livers, respectively. As shown in (■), posttreatment with AG at 1 mmol/L (*arrow*) reversed the LPS-elicited decrease in the baseline bile output. As seen in the *inset*, the decrease in oxygen consumption in the LPS-treated liver was also reversed in concert with a recovery of the bile output. On the other hand, 1 mmol/L N^{ω}-nitro-L-arginine methyl ester did not significantly reverse the LPS-induced decline in the bile output (see *hatched squares and bars*). *Open squares* indicate data collected from the control liver treated with 1 mmol/L AG, showing no significant increase in the baseline bile output. Note that 6-hour–treated liver exhibits a similar reduction of bile output, which is reversibly attenuated by addition of 1 mmol/L AG (see [◎ and ▨]; data represent those measured at 40 minutes). $^*P < .05$ as compared with the control. †$P < .05$, showing a significant recovery as compared with the LPS-treated group. #$P < .05$ as compared with the control. $^{**}P < .05$ as compared with the LPS-treated group.

The anticholestatic effects of AG were also observed when the livers were perfused in the absence of TC. The baseline bile output in the LPS-pretreated liver perfused without TC was significantly lower than that in the control liver. However, the LPS-elicited decrease in the baseline bile output was smaller, being limited to approximately a 15% reduction. In addition, posttreatment with AG at 1 mmol/L reversed the decreased baseline output with marginally greater extents. These findings suggest that LPS treatment down-regulates both bile acid–dependent and –independent fractions of bile output, and the former fraction is preferentially reversed by endogenous NO suppression.

As shown in Fig. 2, the LPS-induced decrease in the baseline bile output coincided with a reduction of the flux in bile salts and phospholipids. Application of 1 mmol/L AG, a blocker of inducible NO synthase, significantly reversed the endotoxin-induced decrease in excretion of these bile constituents, while the same concentration of AG by itself did not significantly alter the baseline bile output and the bile constituents in the control liver. These results suggest that the ability of the LPS-treated liver to excrete bile acids and phospholipids can be reversed by suppression of endogenously generated NO.

We separately examined the effects of MB, a guanylate cyclase inhibitor on the LPS-induced reduction of the bile output. The addition of 250 nmol/L MB in the perfusate significantly stimulated the baseline bile output. On the other hand, supplementation with 1 μmol/L 8Br-cGMP partly repressed the choleretic action of AG. These findings suggest that effects of AG can be ascribed at least in part to its possible action on the suppression of cGMP contents.

Up-Regulation of NO in the Endotoxin-Pretreated Liver. The reversibility of the endotoxin-induced cholestatic response by AG tempted us to examine whether actual NO efflux was elevated in the endotoxin-treated liver. Figure 3 shows concentrations of NO_2^- in the venous perfusate collected from the control and LPS-treated livers. In control liver, the basal NO_2^- flux was approximately 110 nmol/L. On the other hand, the concentration in the liver exposed to 2-hour LPS treatment significantly increased to twofold-greater levels. The increase in NO_2^- was maintained during the entire course of observation. The addition of 1 mmol/L AG significantly suppressed the elevated NO_2^- flux to that in the control level within 20 minutes. This suppression was also maintained until the end of experiments. We also examined

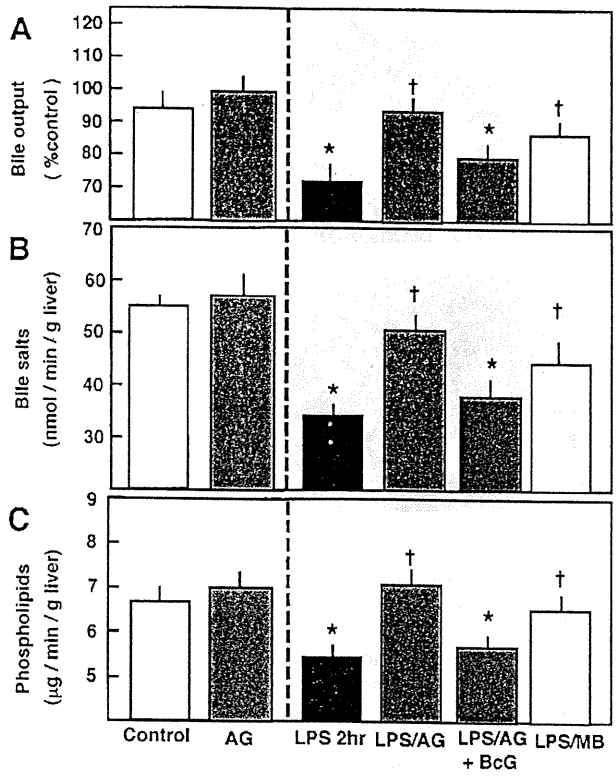

FIG. 2. Effects of LPS pretreatment (2 hours) on the (A) baseline bile output, (B) bile salts, and (C) phospholipid secretion in the perfused liver preparation. Supplementation of AG (1 mmol/L) significantly attenuated the LPS-induced cholestatic changes. 8Br-cGMP (BcG, 1 μmol/L) diminished the action of AG on the LPS-elicited reduction of bile output. MB (250 nmol/L), a guanylate cyclase inhibitor, mimicked in part the repressive action of AG on the LPS-induced reduction of bile output. LPS + AG: n = 11; AG + 8Br-cGMP: n = 10; and MB: n = 10. Data represent mean ± SE of measurements collected at 40 minutes after the start of AG.

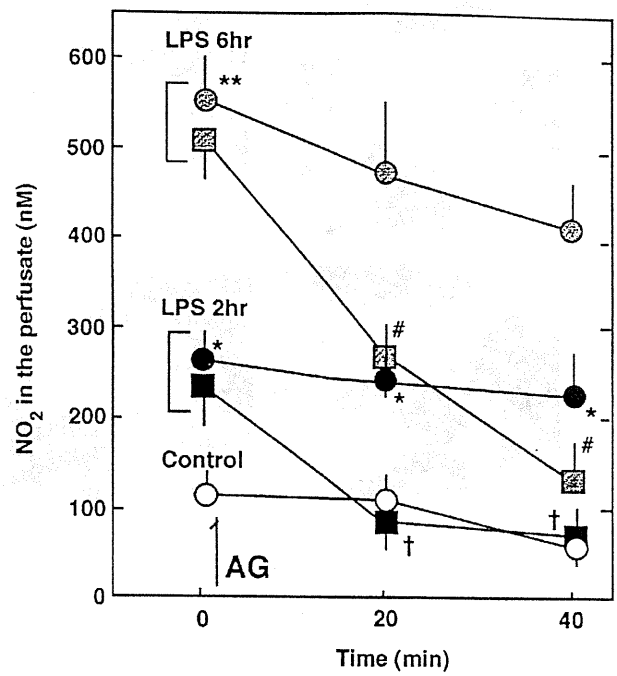

FIG. 3. NO_2^- concentrations in the hepatic venous perfusate collected from the liver exposed to the (● and ■) 2-hour and (▨ and ◎) 6-hour endotoxin treatments. (■ and ▨) The time history of NO_2^- decrease after addition of 1 mmol/L AG. (○) Data collected from the control. Note that the baseline level of NO_2^- increased with longer periods for the LPS treatment. †$P < .05$ and #$P < .05$ as compared with the corresponding control values.

the changes in cGMP contents in the liver tissue (Table 1). The 2-hour LPS treatment up-regulated the tissue cGMP contents to fivefold higher than the control level. The AG treatment significantly attenuated the LPS-induced increase in the cGMP level. The similar results showing elevation of NO_2^- and cGMP, and its reversal by the AG treatment, were obtained in the liver exposed to the 6-hour endotoxin treatment (data not shown). These results suggest that LPS actually evokes an increase in endogenous NO levels, which can be reversed by posttreatment of the NO synthase inhibitor. On the other hand, treatment with 250 nmol/L MB, which attenuated in part the endotoxin-induced cholestatic response (Fig. 2), abolished the cGMP levels in the endotoxin-treated liver.

LPS-Induced Reduction of ATP Contents and Its Reversal by AG. Because the endotoxin treatment preferentially suppressed the bile acid–dependent fraction of the bile output, which is known to require energy-dependent processes, we attempted to find whether the hepatic ATP levels were altered by LPS through the NO-mediated mechanisms. The right-hand portions of Table 1 show the time history of the tissue ATP level among experimental groups studied. In the liver exposed to the 2-hour LPS treatment, the ATP contents were markedly lowered, being approximately 57% of the control level. Upon administration of 1 mmol/L AG, the ATP levels were significantly improved, reaching to the control level. Such a recovery of the ATP levels was not observed when MB was administered. These results suggest that the decrease in tissue ATP contents in the LPS-pretreated liver can be reversed by suppression of endogenously generated NO.

LPS-Induced Mitochondrial Dysfunction Assessed by Rh Microfluorography. The observation showing recovery of the LPS-induced decrease in ATP contents and oxygen consumption by AG led us to examine the possibility that NO overproduction can influence mitochondrial function in hepatocytes, and thereby functionally suppress oxidative phosphorylation.

TABLE 1. LPS-Induced Changes in Tissue Contents of cGMP and ATP and Effects of AG and MB

Group	Tissue cGMP Contents (pmol/g liver)	Tissue ATP Contents (μmol/g liver)
Control	5.7 ± 0.4	1.63 ± 0.12
LPS (2 h)	26.9 ± 0.5	0.91 ± 0.04*
LPS + AG (1 mmol/L)	9.0 ± 1.4	1.30 ± 0.16†
LPS + MB (250 nmol/L)	ND	0.94 ± 0.04

NOTE. Data represent mean ± SE of six to seven measurements using the samples collected at 20 minutes after the start of perfusion in the absence or presence of AG or MB. Note that posttreatment with AG significantly lowered cGMP contents and improved tissue ATP levels.

Abbreviation: ND, not detectable.

*$P < .05$ and †$P < .05$ as compared with the control and the LPS-treated groups, respectively.

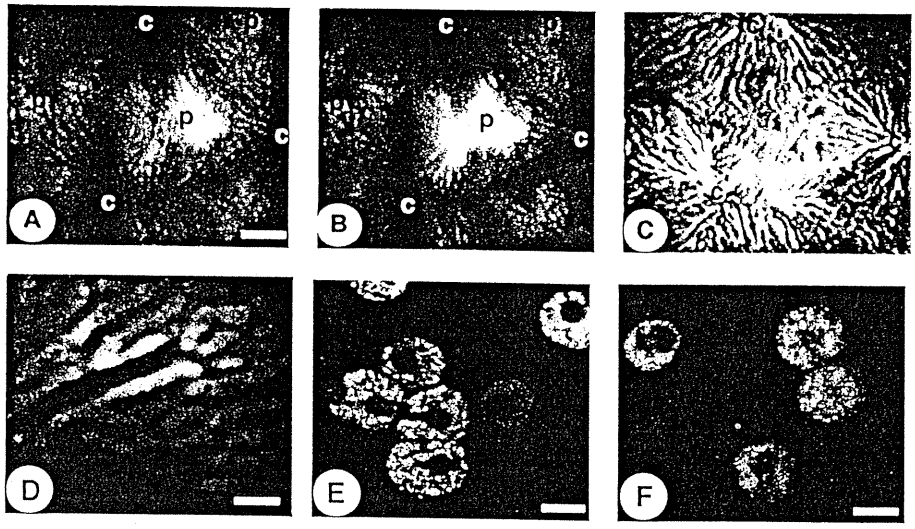

FIG. 4. Intrahepatic Rh microfluorographs in the control perfused liver. (A) A representative picture showing intrahepatic Rh fluorescence at the start of measurements. (B) The fluorograph in the same microscopic field at 40 minutes after the start of experiments. During this period, the buffer containing 0.2 μmol/L Rh was continuously perfused to equilibrate the dye loading. (C) Labeling of sinusoidal capillaries by the fluorescein isothiocyanate–albumin injection to confirm the state of perfusion at the end of experiments. *Bar* in (A) = 100 μm. P, periportal portion; C, centrilobular portion. (D) A representative fluorescence image at higher magnification. *Bar* = 50 μm. (E) Rh-loaded cultured hepatocytes isolated from the control liver. (F) Rh-loaded cultured hepatocytes isolated from the liver exposed to the 2-hour endotoxin treatment. *Bar* = 20 μm in (E) and (F).

To this end, Rh-assisted digital confocal microfluorography was performed. Figure 4 shows laser-scanning microfluorographs in the control perfused liver loaded with Rh. The fluorochrome was loaded panlobularly but with an intralobular gradient (Fig. 4A and 4B). As judged by microangiography by the injection of fluorescein isothiocyanate albumin (Fig. 4C), the areas preferentially stained with Rh were in periportal regions as reported previously.[20,23] The microfluorograph captured under high magnification (40× in objective lens) revealed that a majority of the fluorescence was derived from a cytoplasmic compartment of the parenchymal hepatocytes (Fig. 4D). Furthermore, in cultured hepatocytes isolated from the control liver, the intracellular distribution of Rh exhibited typical multiple and scattered patterns (Fig. 4E). Such features of the intracellular Rh distribution were also well maintained in the cells isolated from the liver undergoing the 2-hour endotoxin treatment (Fig. 4F). Taken together with the previous report showing preferential binding of Rh to mitochondrial inner membrane *in vitro*,[24] these findings suggest that the intracellular Rh localization corresponds to mitochondria in the control and endotoxin-pretreated hepatocytes, as well as under the current experimental conditions.

Using the same protocol for the Rh loading, the microfluorographs in the LPS-pretreated liver were obtained and served as samples for quantitative analysis of mitochondrial function. As shown in Fig. 5, and also shown by quantitative analysis in Fig. 6, the baseline Rh fluorescence intensities became lower than those in the control among the entire lobules. The administration of AG evoked a rapid recovery in the baseline Rh fluorescence in both periportal and pericentral regions (Fig. 5B), indicating that the LPS-induced reduction of the Rh_{app} values is a reversible event.

The Rh_{app} values in different portions of the lobules were quantitatively estimated and were compared among the

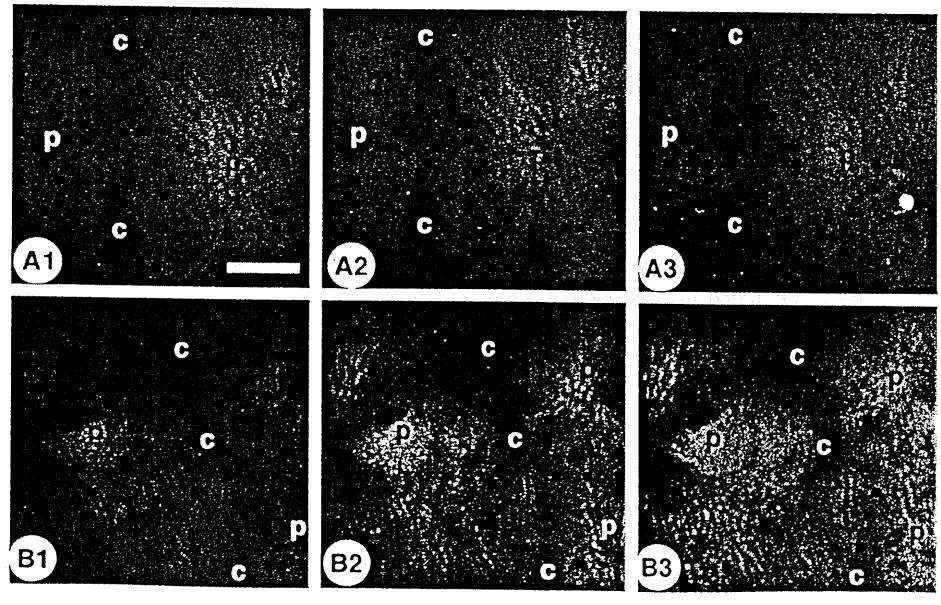

FIG. 5. Time history of the intrahepatic Rh images in the LPS-pretreated perfused liver. LPS administration was completed 2 hours before the start of the liver preparation. (A1-A3) LPS treatment alone. (B1-B3) LPS plus additional application of AG at 1 mmol/L. Fluorographs represent those captured every 20 minutes after the start of *ex vivo* perfusion. *Bar* = 100 μm. P, periportal portion; C, centrilobular portion.

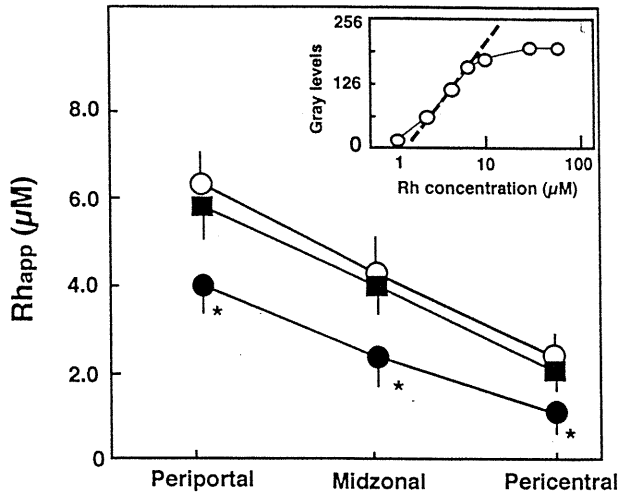

FIG. 6. The intensities of the basal Rh fluorescence measured at the surface of the control and endotoxin-treated livers. As seen in the *inset*, there is a linear correlation between the Rh concentrations (1-10 μmol/L) in the solutions and gray levels measured on a computer-assisted image analyzing system. In the *inset*: (○) mean values of four separate experiments using the Rh-containing solution. Based on this calibration line, the gray-level intensities in different portions of the liver surface were translated into apparent Rh concentrations (Rh_{app}), indicating given concentrations of Rh solutions that generate the same gray-level intensities as those in the liver surface *in situ*. (○) and (●) Data collected from the control and endotoxin-pretreated livers, respectively. These data are mean ± SE measured at 15 to 20 different lobules from five separate experiments. (■) Data from the LPS-pretreated livers that were perfused with the buffer containing 1 mmol/L AG for 20 minutes and then loaded with 0.8 μmol/L Rh for 10 minutes in the presence of AG. The data are mean ± SE measured at 10 different lobules from three separate experiments.

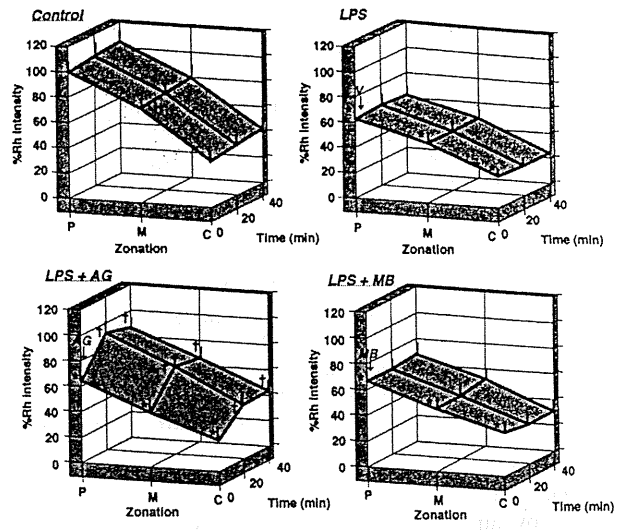

FIG. 7. Semiquantitative analysis of the intrahepatic Rh intensities as a function of the perfusion time and intralobular domains in the control and LPS-pretreated rat livers. The fluorescence intensity measured at 0 minutes in the periportal regions of the control liver was defined as 100 (6.3 μmol/L in Rh_{app}, as shown in Fig. 6), and other measurements were normalized by this value. Note that AG treatment significantly evoked a recovery of Rh fluorescence, suggesting re-energization of mitochondria. V, vehicle. *$P <$ .05 as compared with the values measured in the control liver. †$P <$ .05 as compared with the values measured in the group treated with LPS alone.

groups. As shown in the inset of Fig. 6, the linear relationship between the gray levels and Rh concentrations was established in a range of 1.0 to 10 μmol/L under the current experimental conditions. This calibration line was used to translate the gray levels into the Rh_{app} values. In the liver exposed to the 2-hour LPS treatment, the basal fluorescence intensities exhibited approximately a 35% reduction among the entire portions of the lobules as compared with those in the control liver. When the LPS-pretreated liver was perfused with 1 mmol/L AG and then loaded with Rh, the fluorescence intensity in the parenchyma became greater among the entire lobules, reaching a level equivalent to that observed in the control liver. These results indicate that, in the presence of the NO synthase inhibitor, the LPS-pretreated liver displays similar uptake rates of Rh comparable with that in the control.

Figure 7 represents spatial and temporal alterations in the relative Rh_{app} values (% Rh_{app} as compared with the Rh_{app} in the periportal regions of the control liver at time 0) among the control, and LPS-treated livers perfused with 1 mmol/L AG or 250 nmol/L MB or without these reagents. Upon the AG administration, the periportal and pericentral Rh fluorescence intensities were rapidly recovered within the initial 20-minute perfusion period, exhibiting an approximate 30% increase as compared with those measured before perfusion with this NO synthase inhibitor. After peaking at 20 minutes, the relative Rh_{app} values showed a slight decrease at 40 minutes in the entire portions of the lobules. The AG-induced recovery of the Rh fluorescence was not mimicked by the treatment of 250 nmol/L MB, suggesting that the recovery of the LPS-induced mitochondrial dysfunction by endogenous NO suppression was not reproduced by suppression of cGMP in the liver. We sought to find whether the AG-elicited recovery of the Rh fluorescence is ascribable to the enhanced uptake of Rh from a sinusoidal compartment in sinusoids, rather than to re-energization of mitochondria.

Table 2 shows the effects of 1 mmol/L AG on the Rh_{app} values measured in the LPS-treated liver that was preloaded with 0.8 μmol/L Rh but without supplementation of 0.2 μmol/L Rh. As seen, in the absence of AG, Rh_{app} exhibited an approximate 30% decrease during the 20-minute perfusion in

TABLE 2. Confirmation of the Rh_{app} Reversal by Administration of AG in the LPS-Pretreated Livers Perfused Without a Supplementary Dose of Rh

	Rh_{app} (μmol/L)			
	AG(−)		AG(+)	
Time	Periportal	Pericentral	Periportal	Pericentral
0 min	3.88 ± 0.20	1.60 ± 0.18	3.74 ± 0.17	1.53 ± 0.17
20 min	2.67 ± 0.18	1.12 ± 0.18	4.25 ± 0.17*†	2.07 ± 0.13*†

NOTE. Measurements were performed in the livers that were preloaded with 0.8 μmol/L Rh for 10 minutes but perfused without 0.2 μmol/L Rh during experiments. Data represent mean ± SE of eight measurements from two separate liver preparations. AG was administered right after completing measurements at 0 minutes, when added. Note that the fluorescence recovery by AG is still present in these preparations.

*$P <$ .05 as compared with the data collected from the AG(−) livers at 20 minutes.

†$P <$ .05 as compared with the data measured before the AG administration in the same experiments.

both periportal and pericentral regions, presumably because of the dye excretion into bile. On the other hand, the AG administration significantly increased the baseline Rh_{app} values, indicating that the AG-elicited recovery of Rh_{app} is reproducible irrespective of the presence of the supplementary dose of Rh. At 40 minutes in this protocol, however, the fluorescence in pericentral regions became lower because of the disappearance of the fluorescence from the preparation. These results support a concept that the Rh recovery observed in Fig. 7 results from actual accumulation of the dye in mitochondria, rather than from an increase in the rate of Rh uptake into parenchymal cells.

DISCUSSION

The present study has shown that, in perfused rat liver, LPS induces an impairment of mitochondrial respiration through the mechanism involving an increase in endogenous NO generation. The NO-mediated mitochondrial dysfunction is a reversible phenomenon, because posttreatment with AG, an inhibitor of inducible NO synthase,[24,25] improved decrement of oxygen consumption, ATP synthesis, and mitochondrial membrane potential. The recovery of mitochondrial dysfunction by suppression of NO coincided with enhancement of the bile acid–dependent bile output, suggesting a functional link between the bile-producing ability and mitochondrial energization in the LPS-exposed liver. Uptake, intracellular transport, and excretion of bile salts constitute a sequential multistep mechanism that determines bile output. In addition, bile canalicular contraction is necessary to yield the driving force for bile transport toward the downstream bile duct.[22] These events are known to be energy-dependent[26] and to require Ca^{2+} mobilization.[10,27] According to previous findings revealed by using isolated sinusoidal and canalicular membrane vesicles, mobilization of bile salts across these membrane fractions is enhanced dependently on ATP concentrations in the system.[26] Furthermore, recent investigation has shown that these processes are impaired in endotoxemic rats.[7,8] However, the whole picture of the mechanisms for endotoxin-elicited cholestasis is not fully understood.

The current findings raised at least two possible mechanisms through which overproduction of NO interferes with one of these processes, and thereby inhibits the bile formation. First, through its action on soluble guanylate cyclase, the endotoxin-induced overproduction of NO induces an up-regulation of cGMP, which could in turn suppress bile acid–dependent bile formation.[11] Our findings showing a partial inhibitory effect of 8Br-cGMP on the AG-induced recovery of bile formation suggest that NO-dependent cGMP up-regulation is involved at least in part in the mechanisms for endotoxin-elicited biliary dysfunction. However, the involvement of cGMP-independent mechanisms should also be considered, because inhibition of NO by AG, but not that of cGMP by MB, can reverse the decrease in the bile formation in concert with the recovery of mitochondrial membrane potential and ATP synthesis. These results suggest that overproduction of NO participates in the pathogenesis of the LPS-induced mitochondrial dysfunction through cGMP-independent mechanisms.

Our findings collected from Rh-assisted laser confocal microfluorography suggest that NO-dependent interference with mitochondrial respiration serves as such a mechanism. According to quantitative analysis of changes in intrahepatic mitochondrial membrane potential as a function of time and space in the liver lobules, the 2-hour endotoxin exposure evoked an approximate 35% decrease in Rh fluorescence in the hepatic parenchyma over the entire lobules. Because the decrease in the membrane potential can be estimated as a function of logarithmic value of the relative changes in Rh fluorescence,[19,20] this drop of the fluorescence is equivalent to the voltage changes ranging from 10 to 15 mV. Assuming that mitochondrial membrane potential of normoxic hepatocytes is about 160 mV,[19] this decrease in the hepatocellular mitochondrial potential corresponds approximately halfway toward a total fall of ATP synthesis.[28] This estimation matched well with an actual decrease in ATP contents in the endotoxin-treated liver. The hepatocellular mitochondrial dysfunction is unlikely to result from uncoupling respiration, because the baseline oxygen consumption decreased in parallel with the decreasing membrane potential. These lines of evidence lead us to ask which molecular components associated with mitochondrial respiratory enzymes are responsible for simultaneous suppression of the membrane potential and oxygen consumption by overproduced NO.

Considerable evidence has shown that overproduction of NO evokes irreversible cytotoxic changes among various types of cells and tissues.[3,29] Such biological effects of NO have mainly been understood as a result of its direct interactions with target proteins and enzymes possessing heme and non-heme irons or sulfhydryl residues,[9] as well as its indirect interactions with other oxygen species, including superoxide anions, which in turn generate peroxynitrite, a precursor of NO_2 and hydroxyl radical.[30] Several enzymes serve as possible targets that can interact with NO, and thereby interfere with mitochondrial respiratory function and ATP synthesis: the interactions with Fe-sulfur cluster enzymes such as aconitase, reduced nicotinamide adenine dinucleotide dehydrogenase (complex I), and succinate dehydrogenase (complex II), and those with cytochrome oxidase.[4,31] Recent studies using isolated mitochondria *in vitro* support a concept that cytochrome oxidase accounts for the most plausible molecular target. Cleeter et al. reported that NO can reversibly inhibit cytochrome oxidase and thereby interfere with mitochondrial respiration.[12] In addition, NO is known to reversibly lower mitochondrial inner membrane potential through the mechanism involving cytochrome oxidase.[32] Although the exact molecular mechanisms responsible for the NO-mediated mitochondrial dysfunction are still unknown under the current experimental conditions, the current findings provide evidence that such a reversible inhibition of mitochondrial function by NO actually takes place in the liver as a whole-organ preparation. Moreover, the reversibility of LPS-elicited mitochondrial de-energization and biliary dysfunction leads us to consider the usefulness of selective inhibition of inducible NO synthase as a possible choice of potentially therapeutic methods. Clinical application of this strategy should be awaited until such a biliary dysfunction associated with NO overproduction is actually demonstrated in clinical cases undergoing endotoxemia.

Acknowledgment: The authors thank Dr. Tokio Yamaguchi, Department of Biochemical Genetics, Tokyo Medical and Dental University, for his suggestions.

REFERENCES

1. Harbrecht B, Billiar TR, Stadler J, Demetris AJ, Ochoa JB, Curran RD, Simmons RL. Nitric oxide synthesis serves to reduce hepatic damage during acute murine endotoxemia. Crit Care Med 1992;20:1568-1574.

2. Nishida J, McCuskey RS, McDonnell D, Fox ES. Protective role of NO in hepatic microcirculatory dysfunction during endotoxemia. Am J Physiol 1994;267:G1135-G1141.
3. Billiar TR, Curran RD, Harbrecht BG, Stuehr DJ, Demetris AJ, Simmons RL. Modulation of nitrogen oxide synthesis in vivo: N^G-monomethyl-L-arginine inhibits endotoxin-induced nitrite/nitrate biosynthesis while promoting hepatic damage. J Leukoc Biol 1990;48:565-569.
4. Stadler J, Curran RD, Ochoa JB, Harbrecht BG, Hoffman RA, Simmons RL, Billiar TR. Effect of endogenous nitric oxide on mitochondrial respiration of rat hepatocytes in vitro and in vivo. Arch Surg 1991;126: 186-191.
5. Buttery LDK, Evans TJ, Springall DR, Carpenter A, Cohen J, Polak JM. Immunochemical localization of inducible nitric oxide synthase in endotoxin-treated rats. Lab Invest 1994;71:755-764.
6. Ma T, Ischiropoulos H, Brass CA. Endotoxin-stimulated nitric oxide production increases injury and reduces rat liver chemiluminescence during reperfusion. Gastroenterology 1995;108:463-469.
7. Roelofsen H, Schoemaker B, Ottenhoff R, Jansen PLM, Elferink RPJ. Impaired hepatocanalicular organ anion transport in endotoxemic rats. Am J Physiol 1995;269:G427-G434.
8. Bolder U, Ton-Nu H-T, Schteingart CD, Frick E, Hofmann AF. Hepatocyte transport of bile acids and organic anions in endotoxemic rats: impaired uptake and secretion. Gastroenterology 1997;112:214-225.
9. Moncada S, Pallmer RMJ, Higgs EA. Nitric oxide: physiology, pathophysiology, and pharmacology. Pharmacol Rev 1991;43:109-142.
10. Dufour JFJ, Turner TJ, Arias IM. Nitric oxide blocks canalicular contraction by inhibiting inositol tisphosphate–dependent calcium mobilization. Gastroenterology 1995;108:841-849.
11. Myers N, Grüne S, Jameson HL, Anwer MS. cGMP stimulates bile acid–independent bile formation and biliary bicarbonate excretion. Am J Physiol 1996;270:G418-G424.
12. Cleeter MWJ, Cooper JM, Darley-Usmar VM, Moncada S, Schapira AHV. Reversible inhibition of cytochrome c oxidase, the terminal enzyme of the mitochondrial respiratory chain, by nitric oxide. FEBS Lett 1994;345: 50-54.
13. Adachi Y, Kobayashi H, Kurumi Y, Shouji M, Kitano M, Yamamoto T. ATP-dependent taurocholate transport by rat liver canalicular membrane vesicles. HEPATOLOGY 1991;14:655-659.
14. Yamaguchi T, Wakabayashi Y, Tanaka M, Sano T, Ishikawa H, Nakajima H, Suematsu M, et al. Taurocholate induces directional transport of bilirubin into bile in the perfused rat liver. Am J Physiol 1996;270:G1028-G1032.
15. Sano T, Shiomi M, Wakabayashi Y, Shinoda Y, Goda N, Yamaguchi T, Nimura Y, et al. Endogenous carbon monoxide suppression stimulates bile acid–dependent biliary transport in perfused rat liver. Am J Physiol 1997;272:G1268-G1275.
16. Suematsu M, Goda N, Sano T, Kashiwagi S, Shinoda Y, Ishimura Y. Carbon monoxide: an endogenous modulator of sinusoidal tone in the perfused rat liver. J Clin Invest 1995;96:2431-2437.
17. Misko TP, Schilling RJ, Salvemini D, Moore WM, Currie MG. A fluorometric assay for the measurement of nitrite in biological samples. Anal Biochem 1993;214:11-18.
18. Lust WD, Feussner GK, Barbehenn EK, Passonneau JV. The enzymatic measurement of adenine nucleotides and P-creatine in picomole amounts. Anal Biochem 1981;110:258-266.
19. Lemasters JJ, DeGuiseppi J, Nieminen A-L, Herman B. Blebbing, free Ca^{2+} and mitochondrial membrane potential preceding cell death in hepatocytes. Nature 1987;325:78-81.
20. Suematsu M, Suzuki H, Ishii H, Kato S, Hamamatsu H, Miura S, Tsuchiya M. Topographic dissociation between mitochondrial dysfunction and cell death during low-flow hypoxia in perfused rat liver. Lab Invest 1992;67:434-442.
21. Suematsu M, Suzuki H, Ishii H, Kato S, Yanagisawa T, Asako H, Suzuki M, et al. Early midzonal oxidative stress preceding cell death in hypoperfused rat liver. Gastroenterology 1992;103:994-1001.
22. Oshio C, Phillips MJ. Contractility of bile canaliculi: implications of liver function. Science 1981;212:1041-1042.
23. Suzuki H, Suematsu M, Ishii H, Kato S, Miki H, Mori M, Ishimura Y, et al. Prostaglandin E_1 abrogates early reductive stress and zone-specific paradoxical oxidative injury in hypoperfused rat liver. J Clin Invest 1994;93:155-164.
24. Emanus RK, Grunwald R, Lemasters JJ. Rhodamine 123 as a probe of transmembrane potential in isolated rat liver mitochondria: spectral and metabolic properties. Biochim Biophys Acta 1986;850:436-448.
25. Misko TP, Moore WM, Kasten TP, Nickols GA, Corbett JA, Tilton RG, McDaniel ML, et al. Selective inhibition of inducible nitric oxide synthase by aminoguanidine. Eur J Pharmacol 1993;233:119-125.
26. Müller M, Ishikawa T, Berger U, Klünemann C, Lucka L, Schreyer A, Kannicht C, et al. ATP-dependent transport of taurocholate across the hepatocyte canalicular membrane mediated by 110-kDa glycoprotein binding ATP and bile salt. J Biol Chem 1991;266:18920-18926.
27. Phillips MJ, Oshio C, Miyairi M, Katz H, Smith CR. A study of bile canalicular contractions in isolated hepatocytes. HEPATOLOGY 1982;6:763-768.
28. Anderson BS, Jones DP. Use of digitonin fractionation to determine mitochondrial transmembrane ion distribution in cells during anoxia. Anal Biochem 1985;146:164-172.
29. Curran RD, Billiar TR, Stuehr DJ, Hofmann K, Simmons RL. Hepatocytes produce nitrogen oxides from L-arginine in response to inflammatory products of Kupffer cells. J Exp Med 1989;170:1769-1774.
30. Beckman JS, Beckman TW, Chen J, Marshall PA, Freeman BA. Apparent hydroxyl radical production by peroxynitrite: implications for endothelial injury from nitric oxide and superoxide. Proc Natl Acad Sci U S A 1990;87:1620-1624.
31. Stadler J, Billiar TR, Curran RD, Stuehr DJ, Ochoa JB, Simmons RL. Effect of exogenous and endogenous nitric oxide on mitochondrial respiration of rat hepatocyte. Am J Physiol 1991;260:C910-C916.
32. Schweizer M, Richter C. Nitric oxide potently and reversibly deenergizes mitochondria at low oxygen tension. Biochem Biophys Res Commun 1994;204:169-175.

Carbon Monoxide as a Regulator of Bile Canalicular Contractility in Cultured Rat Hepatocytes

YUICHI SHINODA,[1] MAKOTO SUEMATSU,[1] YOSHIYUKI WAKABAYASHI,[1] TSUNEHARU SUZUKI,[1] NOBUHITO GODA,[1] SHUJI SAITO,[2] TOKIO YAMAGUCHI,[3] AND YUZURU ISHIMURA[1]

This study aimed to examine the mechanism(s) by which carbon monoxide (CO), a product of heme oxygenase reaction, controls the contractility of bile canaliculus (BC) in hepatocytes. When BCs associated with the couplet cells in cultured rat hepatocyte suspension were observed using time-lapse video microscopy, they exhibited periodical contractions with a most-probable interval of 6 minutes under our experimental conditions. The addition of 1 μmol/L zinc protoporphyrin IX (ZnPP), a potent inhibitor of heme oxygenase, to the culture medium elicited a 40% shortening of the interval time together with an increase in intracellular calcium concentrations, while the same concentration of iron protoporphyrin IX did not induce such changes. The production of CO, which was 0.5 nmol/m/10^8cells in the absence of ZnPP, diminished to less than 0.1nmol/m/10^8 cells upon application of ZnPP. The ZnPP-elicited increases in both contractile frequency and intracellular calcium concentrations were attenuated by the addition of 1 μmol/L CO or 50 μmol/L 1,2-bis(2-aminophenoxy) ethane-tetraacetate, a calcium chelator. Clotrimazole or metyrapone, inhibitors of cytochrome P450-dependent monooxygenase activities, also attenuated the ZnPP-induced elevation of the contractile frequency. On the other hand, intracellular cyclic guanosine monophosphate (cGMP) contents were not altered significantly by the application of ZnPP or by CO. These results indicate that CO generated by heme oxygenase controls the BC function by changing intracellular calcium concentrations presumably through a mechanism involving the cytochrome P450 reaction. (HEPATOLOGY 1998; 28:286-295.)

Bile canaliculus (BC) is an intercellular tubular space defined by the apical membranes of adjacent hepatocytes in the liver. Previous studies[1,2] have shown that BCs associated with cultured hepatocytes exhibit autonomous contraction with an interval of several minutes *in vitro*. The contraction process requires intracellular calcium mobilization together with the formation of F-actin in the pericanalicular region,[2] and is thought to be necessary to generate the driving force for bile transport against intramural pressure in the biliary tract. However, little is known about the regulation of autonomous BC contraction. The effects of exogenously applied reagents known thus far are: the frequency of the contraction is increased by taurocholate[3] and endothelin,[4] and is suppressed by cytochalacin B, an inhibitor of actin polymerization,[2] and sodium nitroprusside, a nitric oxide donor.[5]

We have recently found in the liver that the products of heme oxygenase reaction including carbon monoxide (CO) and bilirubin modulate a variety of hepatobiliary functions; zinc protoporphyrin IX (ZnPP), a potent inhibitor of heme oxygenase, eliminated endogenous CO flux and elicited an increase in the vascular resistance concurrent with sinusoidal constriction in the perfused rat liver.[6] The suppression of CO also evoked a significant increase in the bile output in the same preparation,[7] suggesting an active role of this gaseous monoxide in the regulation of biliary function. On the other hand, recent studies suggest that CO regulates contractility and/or motility of various types of cells including vascular smooth muscle cells,[8] hepatic stellate cells,[6] and neutrophils.[9] These observations led us to examine whether CO generated by heme oxygenase modulates the periodicity of BC contraction in cultured hepatocytes. Our findings indicated that CO endogenously produced by HO in hepatocytes controls BC contractility. We have also suggested that effects of CO on the BC contractility are ascribable to its regulatory action on intracellular calcium mobilization through a mechanism involving cytochrome P450–dependent monooxygenases.

MATERIALS AND METHODS

Isolation of Couplet Hepatocytes. Male Wistar rats (240-280 g) allowed free access to laboratory chow and tap water were fasted for 24 hours before killing. After being anesthetized with pentobarbital sodium (40 mg/kg intraperitoneally), the liver was perfused in a single-pass mode with L-15 medium (GIBCO/BRL, Life Technologies, Inc., New York, NY) containing type-IV collagenase (Waco Co., Osaka, Japan) according to a previous method.[1] The liver was excised, mixed with 5 volumes of L-15 medium, and centrifuged at

Abbreviations: BC, bile canaliculus; ZnPP, zinc protoporphyrin IX; cGMP, cyclic guanosine monophosphate; BAPTA-AM, 1,2-bis(2-aminophenoxy) ethane-*N*,*N*,*N*′,*N*′-tetraacetic acid-acetoxymethyl ester; $[Ca^{2+}]_i$, intracellular calcium concentration; fura-2 AM, fura-2-acetoxymethyl ester; TPEN, *N*,*N*,*N*′,*N*′-tetrakis (2-pyridylmethyl) ethylenediamine; SNAP, *S*-nitroso-*N*-acetyl penicillamine.

From the [1]Department of Biochemistry, School of Medicine, Keio University, Tokyo; [2]First Medical Equipment Department, JEOL Trading Co., Tokyo; and [3]Department of Biochemical Genetics, Medical Research Institute, Tokyo Medical and Dental University, Tokyo, Japan.

Received November 12, 1997; accepted April 8, 1998.

Supported by a Grant-in-Aid for Scientific Research from the Ministry of Education, Science, and Culture of Japan, and by grants from Keio University School of Medicine, from Sasakawa Scientific Research Grant, from the Takeda Research Foundation, and in part by Surveys and Research on Specific Diseases from the Ministry of Health on 1996 and 1997.

A preliminary account pertinent to a portion of this work was presented in the Annual Meeting in the American Society for the Study of the Liver Diseases on November 7, 1995, in Chicago, IL.

Address reprint requests to: Yuzuru Ishimura, M.D., Ph.D., Professor and Head, Department of Biochemistry, School of Medicine, Keio University, Tokyo 160, Japan.

0270-9139/98/2802-0002$3.00/0

50g for 5 minutes. Then, a suspension in 50 mL per liver of fresh and cold medium was filtered by nylon mesh and recentrifuged at the same conditions. The cells were inoculated at a concentration of 10^6 cells per milliliter on 35-mm glass-bottom culture dishes (Mat Tek Corp., Ashland, MA), and were kept in an incubator at 37°C under air/CO_2 (95%/5%) for 3 hours before experiments. This 3-hour stabilization period allowed hepatocytes in culture to repair minor morphological damage in their cytoplasmic membrane.[10] The cell viability was 90% to 95% as judged by the Trypan blue exclusion test. This hepatocyte preparation contained approximately 10% of the cells under incompletely separated states, i.e., in couplet, triplet, and cluster states, although the technique was designed to prepare isolated, single hepatocytes. Among them were couplet cells in which BCs were easily visible; an example of such cell pairs chosen by scanning the dish is illustrated in Fig. 1. The BCs were observed through a 100× objective lens with an inverted-type microscope (TMD-300, Nikon, Tokyo, Japan) assisted by a high-resolution low-lag vidicon (C2400-01, Hamamatsu Photonics, Hamamatsu, Japan). The light (150-W Xenon lamp, Sankei Inc., Tokyo, Japan) was filtered by an optical cut-off filter that allowed transmission of light of wavelengths greater than 480 nm. The culture dish and a microscopic stage were kept in a temperature-controlled chamber at 37°C. The dish was continuously superfused with L-15 medium, which was infused at a rate of 0.8 mL/min from the inlet circuit using a Harvard-apparatus pump and was drained from the outlet using a peristaltic pump (F-35, Funakoshi Co., Tokyo, Japan) at the same rate.

Amounts of CO and Bilirubin Produced by the Hepatocytes. To determine the rate of heme degradation in cultured hepatocytes, concentrations of CO and bilirubin were measured as a function of time in the culture medium containing the hepatocytes. The hepatocyte suspension (5×10^6 cells/mL) was incubated in a double-lumen bioreactor (mini PERM, Heraeus Instruments, Inc., Hatz, Germany).[11] As seen in Fig. 2, the bioreactor was composed of a plastic cylinder (16 cm in length and 13 cm in diameter) with two compartments: one was used for the cell suspension (50 mL; Fig.2, part "A," hereafter designated as the cell chamber) and another for the cell-free L-15 medium (450 mL; Fig. 2, part "B," designated as the medium chamber). These compartments were separated by a cellulose membrane that allowed free diffusion of molecules smaller than 10 kd (e.g., CO; Fig. 2, part "C"). The compartment for the cell-free medium was isolated from the atmosphere by a silicon rubber membrane that guaranteed ample supply of oxygen from air to the medium (a cone-shaped portion designated in Fig. 2 as "D"). The whole reactor was placed on a motor-driven turning device and was rotated at 10 rpm in a CO_2 incubator at 37°C. Under these conditions, CO and conjugated bilirubin that evolved in the cell chamber were diffusable into the cell-free medium across the cellulose membrane, as will be described below. Two milliliters of the medium was collected from the outlet (Fig. 2, part "E"), every hour for 6 hours, and was used to determine both bilirubin and CO.

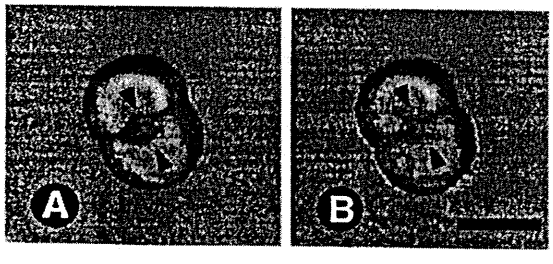

FIG. 1. Representative pictures of a hepatocyte couplet with bile canaliculus. (A and B) A couplet in the maximum diastolic and systolic phases of BC, respectively. Regional domains located between two adjacent *arrows* indicate a single BC in the couplet. *Bar* = 20 μm.

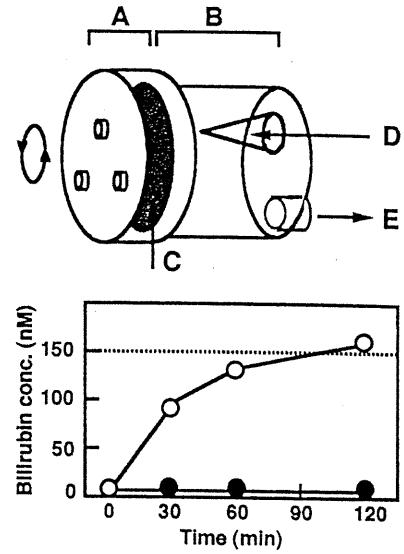

FIG. 2. Schematic diagram of a double-lumen bioreactor for measurements of CO and bilirubin. The *upper portion* illustrates a structure of the bioreactor. (A and B) Chambers for the cell inoculation and for the medium, respectively. (C) A cellulose membrane. (D and E) A silicon-rubber membrane for gas exchange and the outlet for sampling the medium. A *graph* in the lower portion illustrates time history of diffusion of conjugated (○) and unconjugated (●) forms of bilirubin: At time 0, 1.5 μmol/L of conjugated or unconjugated bilirubin was placed in the chamber A. The bilirubin concentrations in the chamber B were measured by enzyme-linked immunosorbent assay assisted by an anti-bilirubin monoclonal antibody, 24G7. Note that conjugated bilirubin reaches equilibrium within 1 hour over the whole chamber, while unconjugated bilirubin is not allowed to diffuse into the medium chamber.

CO in the sample medium was determined by myoglobin-assisted spectrophotometry as described elsewhere.[6] Bilirubin produced by the hepatocytes was also determined by an enzyme-linked immunosorbent assay (ELISA) using two different monoclonal antibodies: 24G7, which recognizes both conjugated and unconjugated bilirubins, and 5M2, which recognizes specifically unconjugated bilirubin.[6,12] These methods allowed us to quantitatively examine bilirubin IXα, the heme-degrading product specifically generated by heme oxygenase.[12] We first examined whether diffusion of the conjugated bilirubin from the cell chamber to the medium chamber across the cellulose membrane could differ from that of the unconjugated form. To that effect, either glucuronyl-conjugated or -unconjugated bilirubin was added first in the cell chamber at 1.5 μmol/L, and time history of the bilirubin concentrations in the medium chamber was determined using the samples collected from the outlet E: if the bilirubin applied in the chamber A can freely diffuse into chamber B without being absorbed to the membrane, its concentration should reach about 150 nmol/L. As seen in the *inset* of Fig. 2, the conjugated bilirubin was able to diffuse into the medium chamber without being entrapped in the cell chamber, inasmuch as the concentration in the medium became about 150 nmol/L within 1 hour after the bilirubin application. On the other hand, the diffusion of unconjugated bilirubin across the membrane appeared to be little, if any, because the bilirubin was detectable neither by 24G7- nor by 5M2-assisted immunoassay system. These results indicate that a major fraction of bilirubin measurable in the medium chamber is the conjugated form released from the cultured cells and not the unconjugated form, which was not allowed to diffuse across the membrane. In the present study, we therefore used the 24G7-assisted enzyme-linked immunosorbent assay to determine concen-

trations of conjugated bilirubin as an index of heme degradation in the cultured hepatocytes.

Time-Lapse Video Analysis of Bile Canalicular Contraction. Time history of BC contraction was videotaped using a time-lapse video recorder (AG-6050, Panasonic, Osaka, Japan) at 30 frames per minute. The time period between two adjacent contractions was defined as the interval time of BC contraction.[2] To determine the intervals, the videotapes showing a series of contractions were replayed by a VHS video player (SVO-260, Sony, Tokyo, Japan) at a rate of 30 frames per second. In each set of experiments, more than 20 pairs of couplets isolated from 8 to 10 livers were observed for 4 to 5 hours. In all experiments, a control recording was performed for 2 hours, and the following time was used to evaluate effects of various reagents in the presence or absence of CO. When administered, 1 μmol/L ZnPP (Aldrich Chemical Inc., Milwaukee, WI) and/or varied concentrations of CO solutions were infused to the circuit for cell superfusion. Although ZnPP is known to directly inhibit the activity of soluble guanylate cyclase,[13] this concentration of ZnPP did not lower cyclic guanosine monophosphate (cGMP) contents in the perfused liver,[7] as well as in cultured hepatocytes as shown later in Results. Effects of 1 μmol/L hemin, iron protoporphyrin IX, were also tested. Separately, 50 μmol/L 1,2-bis(2-aminophenoxy)ethane-*N*,*N*,*N*′,*N*′-tetraacetic acid-acetoxymethyl ester (BAPTA-AM) (Molecular Probes, Eugene, OR),[14-16] a membrane-permeable precursor of BAPTA, a calcium chelator, was added to the dishes at 3 minutes before the start of ZnPP administration. We also examined the effects of clotrimazole and metyrapone, inhibitors of cytochrome P450-dependent eicosatrienoic acid epoxygenase,[17] on ZnPP-elicited changes. The CO solution was prepared from the CO-saturated solution by diluting it with the L-15 buffer. The final concentrations of CO were checked using myoglobin-assisted spectrophotometry as described previously.[6]

Serial Analysis of the Canalicular Space. Using the replayed videotapes showing the BC contractions in BCs, the phase-contrast images of each couplet were stored every 20 seconds from 40 minutes before the start to 40 minutes after the ZnPP application. These images were digitally processed by an 8-bit image analyzer (Image 1.58/Macintosh Quadra 840AV) for measurements of the area of BC. Time history of alterations in the cross-sectional area of BC was traced as described elsewhere.[18] The BC area was estimated from the replayed videotapes every minute to determine its maximum diastolic and systolic sizes. These videoimages were collected by visualizing the hepatocyte couplets using a 100× oil-immersion objective lens as shown in Fig. 1. The values of canalicular areas were calibrated based on the relationship between the pixel counts and known values of area measurements. The measurements of the canalicular areas in individual couplets were plotted as a function of time over 2 hours that involved a 1-hour control period and a subsequent 1-hour observation after the ZnPP application. As an index of "stroke" volume during a single cycle of BC contraction, we analyzed differences in the space between the maximum diastolic and systolic sizes (ΔS_{BC}). These charts plotting alterations in the BC area as a function of time were also used to establish histograms indicating the most-probable time periods between the adjacent BC contractions, as shown below.

Intracellular Ca^{2+} Concentrations in Hepatocytes. Intracellular calcium concentrations ($[Ca^{2+}]_i$) in cultured hepatocytes were determined by measuring fura-2 fluorescence.[19] Briefly, fura-2 was loaded by the addition of 15 μL of 1 mmol/L fura-2 acetoxymethyl ester (fura-2/AM) (Molecular Probes) and 2 μL of 25% Pluronic F127 (wt/vol), both in dimethyl sulfoxide, into 6 mL of the hepatocyte suspension (1×10^6 cells/mL). After washing twice with the L-15 medium, hepatocytes loaded with fura-2 were resuspended into a modified Ca^{2+}-free Krebs-Henseleit solution containing 20 mmol/L HEPES. A 2-mL portion of the cell suspension was transferred to a quartz cuvette placed in a thermostatically controlled sample compartment of a dual-wavelength spectrofluorometer (CAF-100 Ca^{2+} Analyzer, Nippon Bunko Co., Tokyo, Japan). When necessary, either 1.3 mmol/L $CaCl_2$ or 0.5 mmol/L ethylene glycol-bis(β-aminoethyl ether)-*N*,*N*-tetraacetic acid was added to the cell suspension. The cells were kept at 25°C with stirring for 5 minutes before measurements. Fluorescence intensities of the cell suspension at a wavelength of 505 nm were measured under epi-illumination at 340 nm and 380 nm. After recording the baseline fluorescence, ZnPP was added to the cuvette at a final concentration of 1 μmol/L, and the fluorescence changes were traced for 6 minutes. In a separate set of experiments, a small aliquot of the buffer containing CO was transferred to the cuvette using a gas-tight microsyringe to give a final concentration of 2 μmol/L.

Calcium Concentration in Individual Couplet Hepatocytes. Five microliters of the fura-2/AM solution was added to the 35-mm lysine-coated culture dishes containing 1×10^6 hepatocytes in 1 mL Hanks' solution with calcium (1.3 mmol/L $CaCl_2$; GIBCO). After washing twice, the culture dish was placed on the stage of an inverted microscope (TMD-300, Nikon, Tokyo, Japan), which was equipped with an air-conditioned chamber at 37°C. The cells were observed through a 40× oil-immersion quartz objective lens, and their microfluorographs were visualized by a multicolor digital fluorescence imaging system (Quanti Cell-700, Applied Imaging/JEOL, Tokyo, Japan). This system allowed us to visualize microfluorographs under epi-illumination at 340 nm and those at 380 nm alternately with desired exposure time and intervals that were programmed in advance and automatically controlled. The exposure time to obtain a single frame was fixed to 40 ms. Four serial frames were recorded with the 40-ms interval to obtain an individual averaged frame at 340 nm. Immediately after completing such processes to record a 340-nm fluorograph, the same procedures were repeated to record a 380-nm fluorograph. These microfluorographs were digitally processed, and the ratio image was automatically displayed on a television monitor. The ratio images were recorded every 5 seconds for 8 minutes. Data calibration was performed using fura-2–free acid as described elsewhere.[20] The fresh culture medium was infused continuously from the inlet glass tube into the dish (0.8 mL/min) under draining the medium at the same speed. The same inlet was also used to apply the CO-containing solution, BAPTA-AM, or clotrimazole. To avoid possible mixing of heavy metals such as Zn^{2+}, which were known to form a fluorogenic complex with fura-2, effects of *N*,*N*,*N*′,*N*′-tetrakis (2-pyridylmethyl) ethylenediamine (TPEN),[21] a membrane-permeable chelator for the heavy metals, on the fura-2 fluorescence in hepatocytes was examined. In these experiments, TPEN was applied on the culture dish at 3 minutes before the ZnPP administration in a final concentration of 50 μmol/L.

Fluorometric Assay of the Activity of Cytochrome P450 Using Cultured Hepatocytes. A fluorometric assay for the mono-oxygenase activities in the cultured cells was performed using 3-cyano-7-ethoxycoumarin, a substrate for the enzyme reaction, according to a previous method[22]: When freshly prepared hepatocytes are incubated with this membrane-permeable reagent, a time-dependent increase in the fluorescence is known to occur in parallel with generation of 3-cyano-7-hydroxycoumarin, a product yielded by the cytochrome P450–dependent deethylation. The isolated hepatocytes suspended in phosphate-buffered saline at 5×10^5 cells per milliliter were incubated in a 96-well plate with 15 μmol/L of 3-cyano-7-ethoxycoumarin in the presence or absence of 1 μmol/L ZnPP, 1 μmol/L clotrimazole, or varied concentrations of CO. The increase in the 3-cyano-7-hydroxycoumarin–associated fluorescence at 450 nm was monitored time-dependently under illuminating an excitation light at 405 nm using a multiplate fluorescence reader (Luminescence Spectrometer LS50B, Perkin Elmer, Foster, CA). Separately, the fluorescence intensities were calibrated with phosphate-buffered saline containing varied concentrations of 3-cyano-7-hydroxycoumarin. The apparent activity of the monooxygenases in hepatocytes was determined by using the calibration lines, and was expressed as the amount of 3-cyano-7-hydroxycoumarin generated per minute per 1×10^6 cells.

cGMP Contents in Hepatocytes. A 9-mL portion of the hepatocyte suspension incubated in L-15 medium for 2 hours was incubated

with 0.5 mmol/L 3-isobutyl-1-methylxanthine, an inhibitor of phosphodiesterase, for 10 minutes. The cells were then treated with the medium containing desired concentrations of CO, 100 μmol/L *S*-nitroso-*N*-acetyl penicillamine (SNAP) (Intermedical Inc., Tokyo, Japan), or 1 μmol/L ZnPP for 30 minutes at 37°C. The cell pellet was obtained by centrifuging the suspension at 1,000 rpm for 5 minutes at 4°C. The pellet was mixed with 5% trichloroacetic acid and followed by sonication. The samples were centrifuged at 3,000 rpm for 10 minutes at 4°C to collect supernatants, which were subsequently mixed and shaken with water-saturated ethylether. After centrifugation at 3,000 rpm for 10 minutes at 4°C, the ether layer was carefully removed by aspiration to collect the lower water layer. These procedures were repeated three times, and the water layers served as samples for cGMP measurements. The cGMP contents in the samples were determined by an enzyme-linked immunoassay using a commercial assay kit (RPN226, Amersham, Little Chalfont, Buckinghamshire, England).

Statistical Analysis. Differences in median values and standard deviations of histograms showing the frequency profiles of BC contractions were compared among the groups using the nonparametric Wilcoxon's signed ranking test and Kolomogolov-Smirnov test, respectively.[23] Other statistical differences were evaluated by one-way ANOVA with Fisher's multiple comparison test. The values smaller than 0.05 were considered significant. All data were represented by means ± SD.

RESULTS

Generation of CO and Bilirubin in Cultured Rat Hepatocytes. Accumulation of CO and bilirubin in the culture medium of rat hepatocytes was examined as a function of time to evaluate the ability of isolated hepatocytes to degrade endogenous heme. As seen in Fig. 3, concentrations of CO in the medium increased in a time-dependent manner during the 6 hours of our entire experiments. The rate of CO production was fastest in the initial 2-hour period, being 30 nmol/h/10^8 cells, in agreement with our data described elsewhere.[24] The CO concentrations then increased gradually in the following 4 hours. The rate of bilirubin excretion was also time-dependent: During the initial hour, the rate of bilirubin excretion was about 22 nmol/h/10^8 cells, which was about 70% of the CO flux in the same period. The bilirubin flux

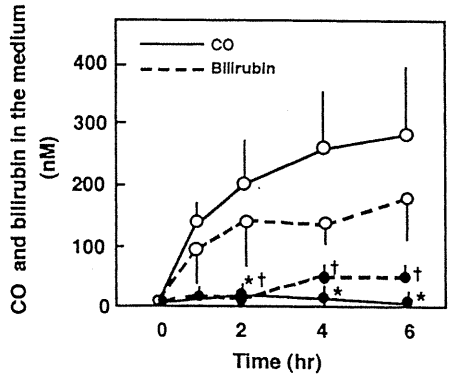

FIG. 3. Time history of concentrations of CO and bilirubin in the culture medium of hepatocytes. *Solid* and *broken* lines denote concentrations of CO and bilirubin, respectively. (○) and (●) denote data obtained with hepatocytes in the absence and presence of 1 μmol/L ZnPP, respectively. Data represent means ± SD of six separate experiments. *$P < .05$ as compared with the control CO concentrations. †$P < .05$ as compared with the control bilirubin concentrations.

then decreased to about half of the initial value at 2 hours and slowly declined in the following 4 hours. Considering the data shown in Fig. 2, differences in concentrations between CO and bilirubin appeared to result from little diffusion of unconjugated bilirubin released from the cells into the medium chamber. When 1 μmol/L of ZnPP, a heme oxygenase inhibitor, was added to the hepatocytes, secretions of both CO and bilirubin from the hepatocytes were almost abolished, as shown in the bottom portion of Fig. 3. These results provide evidence that CO is actually produced in cultured hepatocytes through the heme oxygenase reaction.

Suppression of Endogenous CO Generation Affects the Frequency of BC Contraction. Figure 4 illustrates representative histograms showing the intervals of BC contraction in cultured hepatocyte couplets. Time-lapse video microscopy revealed that BCs in the couplets repeated intermittent contractions for more than 4 hours under the current experimental conditions in the absence of ZnPP. The most frequent interval time between two adjacent BC contractions among these cells was approximately 6 minutes (Fig. 4A), and means ± SD values of the individual intervals were 7.8 ± 3.7 minutes, as described in Table 1. These results were in good agreement with the previous observation by Oshio and Phillips.[1]

To examine effects of suppression of endogenous CO generation on the periodicity of BC contraction, the cell suspension was exposed to ZnPP at 1 μmol/L, the concentration that blocked endogenous heme degradation almost completely, as shown in the experiments in Fig. 3. Following the ZnPP application, the most probable interval in the couplets became 3 to 4 minutes (Fig. 4B), and the mean interval time was 5.5 ± 2.6 minutes, representing approximately a 35% shortening. In the presence of 1 μmol/L CO, the ZnPP-elicited shortening of the interval time was not observed (Fig. 4C). We then examined effects of the application of 1 μmol/L hemin, an iron-centered protoporphyrin IX, which did not elicit the shortening of the interval time (Fig. 4D). Additionally, we studied effects of 1 μmol/L bilirubin on the ZnPP-elicited contractile changes, in which the most-probable interval time was 4 minutes, indicating no significant changes as compared with the ZnPP-treated group (data not shown). Taken together, these results suggest that suppression of endogenous CO generation by heme oxygenase enhanced the contractile activity of BCs.

We further evaluated concentration-dependent effects of CO on the interval time. One micromole per liter of CO *per se* did not evoke any significant difference in the intervals as compared with the control, presumably because of a large standard deviation (Fig. 4E). However, the difference became evident in response to 2 μmol/L CO; the mean value of the intervals was significantly elongated to greater than 11 minutes (Fig. 4F). The effects of this concentration of CO appeared to be reversible, inasmuch as the removal of CO from the superfusion buffer repressed the increasing interval time (data not shown). Furthermore, application of 20 μmol/L CO evoked disappearance of autonomic BC contraction in concert with a marked enlargement of the canalicular area as described below. Under these circumstances, we did not observe the recovery of BC contraction in response to the CO removal from the culture medium. These results indicate that exogenously applied CO elongates the intervals of BC contractions.

Because intracellular free calcium mobilization has been reported to be a prerequisite to the bile canalicular contrac-

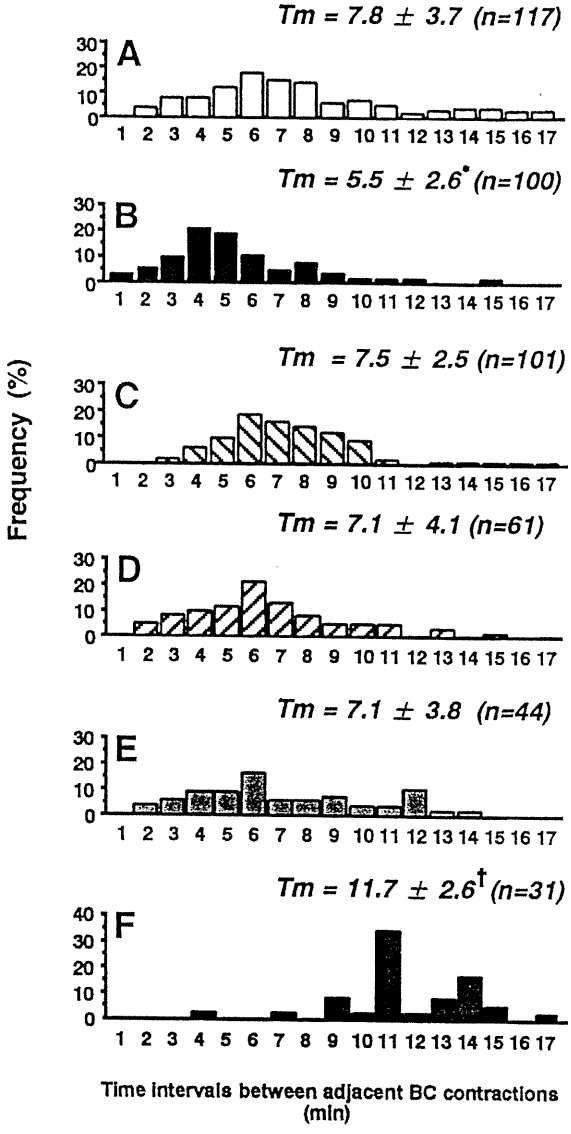

FIG. 4. Effects of ZnPP, CO, and iron protoporphyrin IX (FePP) on the frequency of autonomous BC contractions in hepatocyte couplets. The *horizontal and vertical axes* indicate the intervals between adjacent BC contractions (minutes) and relative frequency of the contraction with specific time intervals (%), respectively. (A) Control; (B) 1 μmol/L ZnPP; (C) 1 μmol/L ZnPP and 1 μmol/L CO; (D) 1 μmol/L FePP; (E) 1 μmol/L CO alone; (F) 2 μmol/L CO alone. A significant difference in the mean values was observed between the control and ZnPP-treated groups (*$P < .05$) as well as between the control and the group treated with 2 μmol/L CO (†$P < .05$), as assessed by one-way ANOVA.

tion,[25] we examined effects of a membrane-permeable calcium chelator, BAPTA-AM, on the autonomous BC contraction (Table 1). As seen, pretreatment with 50 μmol/L BAPTA-AM significantly attenuated the ZnPP-elicited shortening in the contractile intervals. The result suggests requirement of intracellular Ca^{2+} mobilization in the enhancement of BC contraction.

In the next series of experiments, we inquired whether inhibitors of cytochromes P450 mimicked the inhibitory action of CO on the ZnPP-elicited enhancement of BC contraction, because CO is known to inhibit the enzyme activity by binding to the heme moiety: It is well known that CO combines with the ferrous heme proteins but not with ferric ones. In the liver, cytochromes P450, but not other heme enzymes such as cytochrome c oxidase and catalase, are known to be in a ferrous state under ordinary metabolic conditions.[26] Clotrimazole, an inhibitor of cytochrome P450–dependent monooxygenases, was thus applied at 1 μmol/L and significantly attenuated the ZnPP-induced shortening of the time interval for BC contraction (Table 1). Similar suppressive effects on the ZnPP-induced enhancement of BC contraction were observed with 10 μmol/L metyrapone, another inhibitor of the cytochrome P450 enzymes.

Inhibitory Effects of CO on Cytochrome P450–Dependent Monooxygenase Activities in Cultured Hepatocytes. The observation that inhibitors of cytochrome P450–dependent monooxygenases mimicked suppressive effects of CO on BC contractility tempted us to examine whether micromolar levels of CO could actually inhibit cytochrome P450–associated reactions in the cultured hepatocytes. We therefore examined effects of ZnPP, CO, and clotrimazole on cytochrome P450–dependent deethylation of 3-cyano-7-ethoxycoumarin in cultured hepatocytes by measuring the time-dependent increase in the generation of 3-cyano-7-hydroxycoumarin, the fluorescent product of the enzyme reaction (Fig. 5). As seen in a solid calibration line in the *inset*, there was a linear correlation between the concentrations of 3-cyano-7-hydroxycoumarin and the fluorescence intensities. In the presence of 1 μmol/L ZnPP in the cell-free buffer, the calibration line was shifted toward the left as indicated by a broken line, indicating smaller fluorescence with the same concentration of 3-cyano-7-hydroxycoumarin as compared with that in the control. Clotrimazole or CO did not exhibit such a color-quenching effect (data not shown). We therefore determined the enzyme activities in the control, clotrimazole-treated, and CO-treated cells, and those in the ZnPP-treated cells based on the solid and broken lines, respectively.

The results thus obtained indicated that cultured hepatocytes can catalize 3-cyano-7-ethoxycoumarin approximately at a rate of 7 pmol/min/10^6 cells (Fig. 5). Application of 1 μmol/L ZnPP induced about a 5% elevation of the activity, but without statistical significance. On the other hand, CO exogenously applied at micromolar levels significantly inhib-

TABLE 1. Effects of BAPT-AM, an Intracellular Calcium Chelator, and Inhibitors of Cytochromes P450 on the ZnPP-Induced Shortening of the Time Intervals for BC Contraction

Groups	Interval Time (min)	Number of Observation
Control	7.8 ± 3.7	117
1 μmol/L ZnPP	5.5 ± 2.6*	100
1 μmol/L ZnPP + 50 μmol/L BAPT-AM	7.6 ± 5.2†	100
1 μmol/L ZnPP + 1 μmol/L clotrimazole	7.7 ± 2.8†	41
1 μmol/L ZnPP + 10 μmol/L metyrapone	7.6 ± 4.1†	41

NOTE. Data represent means ± SD of measurements from the given number of BC contractions recorded in at least six different couplets.

*$P < .05$ as compared with the control value.

†$P < .05$ as compared with the data in the ZnPP-treated group based on one-way ANOVA analysis combined with Fisher's multiple comparison test.

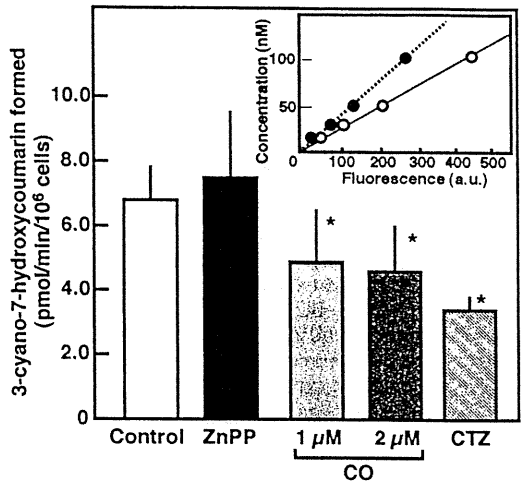

FIG. 5. Inhibitory effects of CO and clotrimazole on cytochrome P450–dependent deethylation of 3-cyano-7-ethoxycoumarin in cultured rat hepatocytes. A final concentration of clotrimazole (CTZ) or ZnPP was 1 μmol/L. The *inset* illustrates calibration lines of known concentrations of 3-cyano-7-hydroxycoumarin, a product of the enzyme activity as a function of the fluorescence intensities expressed as arbitrary units (a.u.). Note that the control calibration line (*solid line*) is shifted to the left in the presence of 1 μmol/L ZnPP, because of its color-quenching action (*broken line*). The data in the ZnPP-treated cells were therefore calibrated based on the *broken line*, while those in other groups were based on the *solid line*. *$P < .05$ as compared with the control.

ited the activity of the cytochrome P450 reaction: 2 μmol/L of CO induced a 40% inhibition of the enzyme activity. Such an inhibitory action on the enzyme activity was also observed under treatment with 1 μmol/L clotrimazole, displaying a 70% inhibition. These results suggest that CO at concentrations used in the present study can actually attenuate the activity of cytochromes P450–dependent monooxygenases.

Effects of ZnPP on the BC Area and Contractile Frequency. Figure 6 illustrates representative data showing the effects of ZnPP on the alterations in the BC area as a function of time. Application of ZnPP at 1 μmol/L induced a significant reduction of stroke changes in the area (Fig. 6A). As shown in Table 2, the ΔS_{BC} value was 3.72 ± 0.30 μm² during the control period before the start of ZnPP application. In response to the ZnPP application, the value exhibited a 40% reduction, suggesting a decrease in the stroke change during a single cycle of the BC contraction. Coapplication with 1 μmol/L CO to the system, however, attenuated the ZnPP-induced ΔS_{BC} decrease significantly (Fig. 6B), suggesting that the ZnPP-induced changes occurred as a consequence of CO suppression.

When the couplets were superfused continuously with 20 μmol/L CO alone for more than 5 minutes, the frequency of BC contractions became decreased and the S_{BC} values in the maximum systolic phase showed a marked elevation, leading to a maximum dilatation of BC (Fig. 6C). Taken together with the current data showing elongation of the interval time elicited by 2 μmol/L CO application, these results indicate that excessive CO application suppresses autonomous contractile activities in BC.

ZnPP-Elicited Increase in $[Ca^{2+}]_i$. The inhibitory effect of BAPTA-AM on the ZnPP-induced activation of BC contraction described above tempted us to examine whether CO suppression by the ZnPP treatment actually influences the intracellular Ca^{2+} concentrations in the couplets. Figure 7 illustrates a representative picture showing alterations in the $[Ca^{2+}]_i$ demonstrated by fura-2–assisted digital microfluorography in rat hepatocyte couplets. As shown, the majority of couplets exhibited a $[Ca^{2+}]_i$ increase that occurred within 2 minutes after the start of ZnPP application, although some couplets exhibited a sustained pattern of $[Ca^{2+}]_i$, while others showed an oscillatory pattern. As a whole, however, the ZnPP application induced a marked increase in the $[Ca^{2+}]_i$ value, as shown in Fig. 8A, illustrating the data collected from more than 20 cell pairs. The ZnPP-induced elevation of $[Ca^{2+}]_i$ was blocked almost completely by pretreatment with 2 μmol/L CO or with 1 μmol/L clotrimazole. When the couplets were pretreated with 50 μmol/L BAPTA-AM, the basal $[Ca^{2+}]_i$ values exhibited approximately a 30% decrease. The $[Ca^{2+}]_i$ values neither increased nor restored the original level upon the application of 1 μmol/L

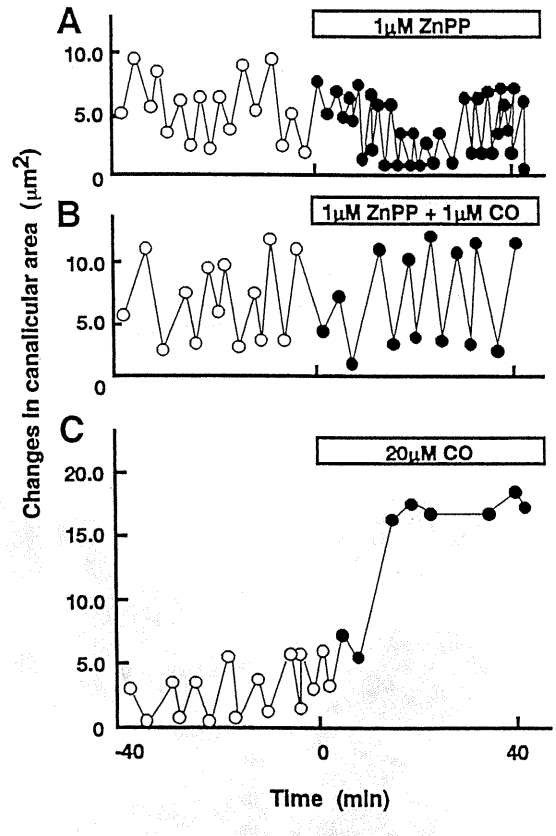

FIG. 6. Effects of ZnPP on temporal alterations in canalicular areas in individual rat hepatocyte couplets. The hepatocyte couplets exhibiting the most-probable contractile intervals of 5 to 7 minutes were chosen for the data analysis. Only those corresponding to the maximum systolic and diastolic phase were plotted on the diagrams based on a series of measurements of SBC, which were performed every 20 seconds from 40 minutes before the start of the ZnPP application. *Trace A*: 1 μmol/L ZnPP. *Trace B*: 1 μmol/L ZnPP + 1 μmol/L CO. *Trace C* illustrates the effects of 20 μmol/L CO, showing the maximum BC dilatation with disappearance of contractile activities.